



รายงานวิจัยฉบับสมบูรณ์

โครงการ

การตรวจคัดกรองโมเลกุลขนาดเล็กที่ยับยั้งโปรติเอสหลัก (3CL^{pro}) ของไวรัสโคโรนาในแมวโดยใช้แบบจำลองทางคอมพิวเตอร์

โดย ผู้ช่วยศาสตราจารย์ สพ.ญ.ดร.ศิรินทร์ ธีระวัฒนศิริกุล

เดือนเมษายน ปี 2562

สัญญาเลขที่ MRG6080067

รายงานวิจัยฉบับสมบูรณ์

โครงการ

การตรวจคัดกรองโมเลกุลขนาดเล็กที่ยับยั้งโปรติเอสหลัก (3CL^{pro}) ของไวรัสโคโรนาในแมวโดยใช้แบบจำลองทางคอมพิวเตอร์

คณะผู้วิจัย

- 1. ผศ.สพ.ญ.ดร. ศิรินทร์ ธีระวัฒนศิริกุล
- 2. ศ.สพ.ญ.ดร.พรทิพภา เล็กเจริญสุข

สังกัด

คณะสัตวแพทยศาสตร์ มหาวิทยาลัยเกษตรศาสตร์ คณะสัตวแพทยศาสตร์ มหาวิทยาลัยเกษตรศาสตร์

สนับสนุนโดยสำนักงานกองทุนสนับสนุนการวิจัย และมหาวิทยาลัยเกษตรศาสตร์

(ความเห็นในรายงานนี้เป็นของผู้วิจัย

สกว.และมหาวิทยาลัยเกษตรศาสตร์ไม่จำเป็นต้องเห็นด้วยเสมอไป)

บทคัดย่อ

รหัสโครงการ: MRG6080067

ชื่อโครงการ: การตรวจคัดกรองโมเลกุลขนาดเล็กที่ยับยั้งโปรติเอสหลัก (3CLpro) ของ

ไวรัสโคโรนาในแมวโดยใช้แบบจำลองทางคอมพิวเตอร์

นักวิจัย: ผศ.สพ.ญ.ดร. ศิรินทร์ ธีระวัฒนศิริกุล คณะสัตวแพทยศาสตร์ ม.เกษตรศาสตร์

E-mail Address: fvetsrth@ku.ac.th

ระยะเวลาโครงการ: 2 ปี (ระหว่างวันที่ 4 เมษายน 2560 ถึง วันที่ 3 เมษายน 2562)

โรคเยื่อบุช่องท้องอักเสบติดต่อในแมวเป็นเชื้อไวรัสโคโรนาซึ่งเป็นไบโอไทป์ที่มีความ ไวรัสโคโรนาในแมวถูกจัดอยู่ในวงศ์โคโรนาวิรีดี และอยู่ในกลุ่มอัลฟาโคโรนาไวรัส ในปัจจุบันยังไม่พบการรักษาหรือตัวยาใด ๆที่จะสามารถลดอาการของโรคได้ การวิจัยในช่วง สิบปีที่ผ่านมามีการนำเทคโนโลยีการสร้างแบบจำลองระดับโมเลกุล และการตรวจคัดกรอง ซึ่งเป็นวิธีการที่สามารถช่วยในการพัฒนายาต้านไวรัส ดังนั้นการวิจัยในครั้งนี้มีวัตถุประสงค์ เพื่อประยุกต์ใช้วิธีการทางคอมพิวเตอร์ในการคัดกรอง เพื่อหาบริเวณแอคทีฟของบริเวณ ช่องว่างที่จับของโปรตีนด้วยโมเลกุลสารเคมีที่หาได้จากฐานข้อมูล การจับกันอย่างจำเพาะ ของโปรติเอสของไวรัสโคโรนาในแมว ซึ่งเป็นโปรตีนที่สำคัญ (FIP3CL protease) ในการเพิ่มจำนวนของไวรัส การใช้คอมพิวเตอร์เพื่อหายาที่เป็นตัวแทน จากในฐานข้อมูล จำนวน 2,389,748 สาร โดยใช้อัลกอริทึม ได้แก่ 1) ซอฟแวร์ออโตด็อก วีนา 2) โกลด์ และ 3) ไอซีเอ็ม สารที่ได้จากการคำนวณทั้งสามซอฟแวร์ จำนวน 86 สาร และทำการเลือก สารที่มีอันดับที่ซ้ำกันทั้งสามซอฟแวร์ จากนั้นคำนวณค่า AUC = 0.742 มีค่าตั้งแต่ 0.742–0.849 สารตัวแทนที่ได้จำนวน 20 สาร จะถูกนำมาทดสอบการยับยั้ง โปรติเอสโดยใช้เชื้อ FIPV strain 79-1146 โดยการทำการแสดงออกของโปรตีนของ FIP3CL protease เพื่อสร้างโปรตีน เอนไซม์ และทำการทดสอบความสามารถในการทำงานของเอนไซม์ โดยมีค่า Km = 8.56±1.15 μM and Vmax = 0.0247 ± 0.00149 µM/sec ตามลำดับ จากนั้นโปรตีนโปรติเอสที่ได้ ถูกนำมาทดสอบการยับยั้งด้วยสารตัวแทน พบว่า สาร 1–6 จะมีค่าความเข้มข้นของสารใน การยับยั้ง (IC₅₀) น้อยกว่า 10 μM การทดสอบ ความเป็นพิษต่อเซลล์และทดสอบ การยับยั้งไวรัสจะนำมาทดสอบด้วยเซลล์เพาะเลี้ยงตาม ลำดับ การตรวจสอบปริมาณของไวรัส จะใช้วิธีการ IPMA และวิธีการอณูชีววิทยา (Realtime qPCR) พบว่าสาร 1, 3, 4, 5 และ 13

มีค่าความเข้มข้นของสารที่มีประสิทธิภาพของการยับยั้ง (EC₅₀) ที่ดีกว่ายาควบคุมซึ่งเป็น ยาต้านไวรัสและยายับยั้งโปรติเอส การจำลองการจับกันของสารตัวแทน 1 กับ FIP3CL protease เพื่อระบุปฏิกิริยาของการจับกันค่อนข้างดี จากผลของการศึกษาทั้งหมด พบว่า สารตัวแทน 1 นั้น ควรจะเป็นสารที่ดีที่สุด ในการยับยั้งการเพิ่มจำนวนของไวรัส โคโรนาในแมว

คำหลัก: การยับยั้งโปรติเอสหลัก, แบบจำลองทางคอมพิวเตอร์, โมเลกุลขนาดเล็ก, ไวรัสโคโรนาในแมว

Abstract

Project Code: MRG6080067

Project Title: Computer-aided virtual screening for small molecules that inhibit

protease (3CL^{pro}) of feline coronavirus

Investigator: Assistant Professor Dr. Sirin Theerawatanasirikul

Faculty of Veterinary Medicine, Kasetsart University

E-mail Address : fvetsrth@ku.ac.th

Project Period: 2 years (4 April 2017 – 3 April 2019)

Feline infectious peritonitis virus (FIPV) is a virulent biotype of feline coronavirus (FCoV) and belongs to the genus Alphacoronavirus within family Coronaviridae. At the present, there is neither an effective treatment nor a convincingly reduction increase for the disease progression. As a decade, the combination of molecular modeling techniques and virtual screening approaches are the powerful tools that can accelerate and guide the development process of antiviral drugs. Therefore, this study aims to apply the computer-aided virtual screening to determine the active site on the viral binding pocket for the available chemical compounds. The specific binding targets to the FIP3CL protease, the main protease, that plays a role in a viral replication cycle. The computer-based approach was utilized for retrieving the new candidate compounds in the available chemical databases (2,389,748 compounds) using the molecular docking algorithms (AutoDock Vina, GOLD and ICM software). The candidate ranked-consensus based on 86 top ranks from the three softwares were evaluated; the AUC = 0.742, with the range from 0.742–0.849. The twenty-top ranks of those compounds were tested for further assays. The FIP3CL protease was derived from FIPV strain 79-1146 using a protein expression system. The enzyme activity was demonstrated. As the results, the Km value was $8.56\pm1.15~\mu\text{M}$ and Vmax were $0.0247~\pm~0.00149~\mu\text{M/sec}$, respectively. Then, the protease inhibitory assay was performed for screening the inhibitory effect of the candidate compounds. The compounds 1-6 had the better IC₅₀ values, which were less than 10 μ M. The candidate compounds were evaluated the cytotoxicity (CC50) using MTS assay. Then, antiviral activity was

tested using the cell-based assay. The results showed that compounds 1, 3, 4, 5 and 13 possessed the better EC_{50} values than the broad-spectrum antiviral drug and the protease inhibitor as determined by using IPMA and realtime qPCR detections. Finally, the MD simulation of FIP3CL-compound 1 complex used to define the interaction using *in sillico* assay with slightly good interaction. From the results of two approaches, the compound 1 was the best compound to inhibit the FIPV replication.

Keywords: Protease inhibition, Computer-aided virtual screening, Small molecules, Feline coronavirus

Executive Summary

Feline infectious peritonitis virus (FIPV) causes a fatal disease in domestic cats in Thailand and worldwide. Currently, no effective vaccine or antiviral drug can inhibit FIP disease progression and transmission. Therefore, the antiviral drugs specific to FIPV is required. Thus, the propose of this research is to search for the candidate anti-FIPV lead compounds from available database and examined their antiviral activities *in vitro*.

To find the new candidate anti-FIPV compounds from the available chemical databases, homology and molecular docking analyze were performed using AutoDock Vina, GOLD and ICM programs. Eighty-six compounds showing a significantly higher AUC ranged from 0.742 to 0.849 were selected. The scoring function was performed from molecular complexes between FIP3CL^{pro} and the top-ranked compounds using three algorithms. As a result, the consensus top-ranked compounds from these algorithms were further tested *in vitro* including protease inhibition and cell-based assays.

To examine anti-protease activity of the compounds, the recombinant FIP3CL^{pro} plasmid was constructed and the FIP3CL^{pro} was produced in *E.coli*. The enzyme activity was tested using the fluorogenic peptides as substrate for the FIP3CL^{pro}. The twenty topranked candidate compounds were tested for protease inhibition assay. The results showed that at least six compounds (compounds 1–6) showed good IC₅₀ values (0–30 μM). These compounds were used for the further cell-based experiment.

To perform cell-based assays, FIPV strain 79-1146 was propagated in the CRFK cells and the infected CRFK cells was detected by immunoperoxidase monolayer assay (IPMA). Cell cytotoxicity (CC_{50}) of each compound on the CRKF cells was evaluated. The result showed that eighteen out of twenty compounds possessed CC_{50} higher than IC_{50} values obtained from the protease inhibition assay.

The antiviral activity of selected compounds was examined by the three experiments consisting of the pre-viral entry, post-viral entry and prophylactic activities. The antiviral effectiveness (EC $_{50}$) was defined as concentration of an active compound that can inhibit 50% CRFK cells from FIPV infection compared with viral infected cell control. In the pre-viral entry assay, the results showed that the EC $_{50}$ of compounds 1, 3, 4, 5 and 13 showed the good inhibition activities (range 1.186–16.24 μ M). The post-viral entry assay demonstrated that the compounds 1, 3, 4, 5, 13 and 18 had the better EC $_{50}$ values (range 2.34–31.951 μ M); in particular, compounds 5, 13 and 18 had better EC $_{50}$ values than those from the pre-viral entry assay. The prophylactic activity showed that compounds 1, 4, 5 and 13 could penetrate into the host cells and had viral inhibitory effect with good EC $_{50}$ values (range 1.998–16.222). The results of protease inhibition and cell-based assays of compound 18 were inaccordant. It had a good antiviral activity in the cell-based assay, but it could not inhibit FIP3CL pro as well.

According to our results, compound 1 displayed good FIP3CL^{pro} inhibition that was found in all assays. Therefore, the complex of FIP3CL^{pro}—compound 1 was selected for a study on the molecular dynamic interaction. In the FIP3CL^{pro} binding pocket, His41 and Cys144 residues were found to form alkyl and hydrogen bonds to the compound 1. The other molecules were also found to interact in the binding pocket with the van der Waals force, alkyl bonds and hydrogen bonds, respectively.

In conclusion, the compound 1 is the most promising protease inhibitor that could prevent the FIPV infection probably by targeting the FIP3CL^{pro}. It is the candidate antiviral lead compound that worth further development to generate therapeutic agents for FIPV and other emerging CoV-associated diseases. The output from this study will be two international publications within Science Citation Index (SCI) of Web of Science.

Introduction

Feline infectious peritonitis virus (FIPV) is a virulent biotype of feline coronavirus (FCoV) and belongs to the genus *Alphacoronavirus* within family *Coronaviridae*. FIPV arises by mutation from the parental enteric form of FCoV called feline enteric coronavirus (FECV) within the infected cats. FIP is a fatal disease in domestic cats particularly multiple cat households in Thailand and worldwide [Manasateinkij et 2009; Pedersen, 2009; Pedersen, 2014b]. FIP is a serious (pyo-) granulomatous disease affecting almost all body systems with protein-rich effusions in body cavities. A progressive, multifocal granulomatous of various organs is the cause of death in cats. Viral particles were observed in the organs of experimental infected healthy cats. The causative agent, FIP virus (FIPV) is a coronavirus (CoV). A severe progression of this disease is over a week to month, which is always the cause of death in young cats [Hartmann, 2005; Pedersen, 2009].

FCoV was divided into 2 biotypes, the virulent biotype FIPV and the enteric biotype (feline enteric coronavirus, FECV) [Pedersen, 2009; Pedersen, 2014b]. FECV is ubiquitous and causes asymptomatic or mild infection of cats. However, it can transmit efficiently via fecal-oral route among cats. In contrast, FIPV refers to as the virulent biotype that causes a lethal systemic granulomatous disease in individual cats [Pedersen, 2009; Pedersen, 2014a; Pedersen, 2014b, Kipar and Mel, 2014]. The viral biology of FIPV quite differs from other viruses, since the transmission is infrequently spread from animal to animal in a horizontal spread. FIPV is still highly infectious when the extracts from infected tissues or fluids from the peritoneum and the thoracic cavity are inoculated into naïve cats. However, FECV is the most common biotype that could be identified in the feces of cats [Pedersen, 2009; Pedersen, 2014a; Pedersen, 2014b, Kipar and Mel, 2014]. This leads to the assumption that transmission among cats in the form of FECV. Transformation of FECV to FIPV may be induced by genetic deletion and/or immune modulation, resulting in the progressive development of FIP disease. In addition to biotype, FCoVs are genetically divided into 2 serotypes: FCoV type I and FCoV type II. Two serotypes of FIPV have different growth characteristics in cell culture and genetic relationship. The serotype II of FCoV has emerged from double recombination between type I FCoV and CCoV. Type II FCoV is much more related to FIPV than the serotype I viruses [Pedersen et al, 2007; Chang et al, 2010].

Epidemics of this disease in the last few years increasingly occurred in the multiple-cat households with high mortality rate [Manasateinkij et 2009; Pedersen 2009,

Foley et al, 1997]. The virus could survive in dry condition up to 7 weeks; in particular, cat-litter boxes are the sole source of viruses and the major mode of transmission is via fecal-oral route [Hartmann, 2005]. For treatment of FIP disease in cats, several strategies have been used to combat this disease. First, the proven inhibitors for other viruses such as HIV-1, hepatitis B and C virus acting on the viral replication were applied experimentally [Hartmann, 2005; Hartmann and Ritz, 2008; Pedersen, 2014a; Hsieh et al, 2010; Kim et al, 2013]. In the second strategy, anti-inflammatory and immunosuppressive drugs were used to inhibit the inflammatory process and reduce clinical signs in cats. The third strategy was the application of non-specific immunostimulants for stimulating the immune system, which aimed to expand the cat's life. In the fourth strategy, combination of anti-viral drugs and immunostimulating drugs has been reported in human viral infection therapy. However, there is no obvious evidence that these strategies were used successfully to cure FIP. Some studies in veterinary research reported the use of inhibitors such as protease and cathepsin B inhibitors, which aimed to inhibit directly to the main protease of coronavirus (3CL^{pro}).

Nelfinavir, the human HIV-1 protease inhibitor, could not inhibit FIPV replication [Hsieh et al, 2010]. Combination of these drugs with other groups of therapeutic agents such as immunosuppressive and immunostimulant drugs could not improve the disease outcome [Hartmann, 2005; Hartmann and Ritz, 2008; Pedersen, 2014a, Kipar and Meli, 2014]. Although ribavirin is a primary drug for hepatitis C treatment in human, it is not useful for FIPV treatment in cat due to high toxicity and the adverse side effects [Weiss et al, 1993]. However, the efficacy of these human antiviral drugs on FIP treatment are unsatisfied. At present, the standard treatment is aimed to prolong life span and improve quality of life, which includes anti-inflammation and supportive treatment [Hartmann and Ritz, 2008; Pedersen, 2014a]. Therefore, it is needed to find the antiviral drugs specific for FIPV treatment.

FIPV is a coronavirus, which is enveloped. The particle is pleomorphic and contains a single-stranded positive sense RNA. The genome of FIPV consists of 30,000 nucleotides and 11 open reading frames (ORFs) encoding structural, non-structural and accessory genes [Pedersen, 2009; Lin et al, 2013; Pedersen, 2014b]. The 5' two third of FCoV genome comprises of the 2 overlapping ORFs, ORF 1a and 1b that encode 2 polyproteins. Translation of ORF1a yields a polyprotein pp1a. At small proportion, ribosomes initiate translation at the beginning of ORF 1a and undergo frame shifting at the junction between ORF 1a and 1b, resulting in a long polyprotein, pp1ab [Pedersen et

al, 2014b, St.John et al, 2015; Wang et al, 2015]. These polyproteins are subsequently and enzymatically cleaved into 16 nonstructural functional proteins (nsp1 to nsp16) mainly involved proteolytic processing and viral RNA synthesis including genome replication and subgenomic mRNA synthesis. The remaining genome contains 9 ORFs that encode 4 structural proteins of spike (S), nucleocapsid (N), membrane (M) and envelope (E) proteins, and 5 accessory proteins (3a–c, 7a and b) [1–4, 14].

Similarly to other CoV viruses, FCoV 3CL^{pro} has two cysteine proteases are the papain-like protease (PL^{pro}) and the 3 chymotrypsin-like protease (3CL^{pro}). The 3CL^{pro} is also known as the main protease (M^{pro}) [Pedesen, 2014b; St.John et al, 2015; Wang et al, 2015; Berry et al, 2015]. Particularly, the 3CL proteases play a pivotal role in viral gene expression, viral replication and life cycle. The highly complex cascade involves the proteolytic processing of replicase polyproteins. Generally, coronaviruses can infect various species of mammals and avian, which are common cause of transient enteritis and respiratory diseases. FIPV is closely related to transmissible gastroenteritis virus (TGEV) in pigs and canine coronavirus (CCoV) [Pedersen, 2009; Pedersen, 2014a; Pedersen, 2014b; Dedeurwaerder et al, 2013; St.John et al, 2015; Wang et al, 2015; Berry et al, 2015].

Coronavirus 3CL^{pro} shares common characteristics in functional and structural properties to the 3C protease or 3CLpro of picornavirus, norovirus and SARs-CoV, respectively [Kim et al, 2013]. In human coronavirus, the 3CL pro has been termed "the Achilles' heel of coronaviruses". It is an attractive target in drug discovery and the 3CL^{pro} of FIPV could be a model to study the candidate antiviral drugs against further emerging CoV-associated diseases, especially the in vitro assay is available in the FIPV system. A development of inhibitors targeting 3CL^{pro} includes pyridine N-oxide derivatives, peptidomimetic analoques, covalent inhibitors and small molecule inhibitors have been evaluated [Berry et al, 2015; Ferreira et al, 2014; Murkherjee et al, 2011]. The protein structure of SARs-CoV 3CL pro was solved by X-ray crystallography as well as nuclear magnetic resonance (NMR). Since the first elucidated crystal structure, twenty crystal structures with enzymes and inhibitors have been reported. These could be used for virtual screening by mimicking the interactions between the database compounds and the active site of SARs-3CL^{pro} as previously reported [Berry et al, 2015, Murherjee et al, 2011, Niu et al 2008]. However, an in vitro cell-based analysis is required to test the inhibitory effect and toxicity of the compounds. Two crystal structures of FCoV 3CL pro have been recently reported [St. John et al, 2015; Wang et al, 2015]. This 3CL pro and complex of peptidomimetic inhibitors, Michael acceptor inhibitor and a metal ion Zn^{2+} have been determined the 3D structure. The $3CL^{pro}$ contains two protomers and each monomer has 3 domains. Domains I and II consists of antiparallel β -barrels and the domain III contains five α -helices [St. John et al, 2015; Wang et al, 2015]. The reported compounds react in the binding pocket in the active site of $3CL^{pro}$ located between domains I and II. The crystal of the complex structure could provide fundamental structure for *in silico* analysis and the design of novel antiviral drugs targeting $3CL^{pro}$ of FIPV and other related CoV important in Veterinary and Medical researches.

As following the emerging and fatal human viruses, the severe acute respiratory syndrome (SARs) and Middle Eastern respiratory syndrome (MERS) posted a significant threat on human and caught dramatically interest by medical and molecular biological researchers [Berry et al, 2015]. In addition, these viruses belong to the subfamily *Coronavirinae*, family *Coronaviridae*, similar to FIPV. These viruses then share common characteristics and biology including genome organization and gene expression. Thus, animal coronavirus such as FIPV that can be cultured in cell lines could be a good study model for the fatal emerging viruses in human.

Propose of this research is to utilize the molecular modeling techniques and virtual screening approaches to search for the candidate anti-FIPV lead compounds from available database. This approach can avoid the investments on agents or drugs that do not present the suitable properties and will reduce the failure on down-stream *in vitro* and *in vivo* assays and the later stages of clinical tests. In addition, the compounds will then be tested for antiviral activity *in vitro*. This study may provide useful precursors and information for further development of the potential therapeutic agents against FIP and other emerging CoV-associated diseases.

Objectives

The aim of this study is to search for a candidate antiviral lead compounds that can inhibit FIPV replication in vitro.

Objectives

- To screen the candidate small-molecular compounds from available and purchasable databases that bind to 3CL^{pro} of FCoV specifically and with high affinity by the computer aided screening
- 2. To evaluate the candidate compounds for their inhibitory activity against FIPV replication in vitro using cell-based assay.

Scope of research

The specific works are corresponding to the research objectives as follows **Objective 1**: To screen the candidate small-molecular compounds from available and purchasable databases that bind to 3CL^{pro} of FCoV specifically and with high affinity by the computer aided screening

Specific works:

- 1. Retrieve crystal structures of FIPV 3CL^{pro} from PDB databases and prepare the structures for virtual screening
- 2. Process the simulation structure by removing sulfate ion and water and adding H-bond
 - 3. Set up the library of chemical compounds from available databases
 - 4. Dock the ligand onto the structural file and visualize using molecular software
- 5. Calculate the force fields between the interacting complex using computer software

Objective 2: To evaluate the candidate compounds for their inhibitory activity against FIPV replication in vitro using protease inhibitory and cell-based assay

Specific works:

- 1. Construction of FIP3CL protease and inhibitory assay.
- 2. Propagate and titrate virus stock
- 3. Cytotoxicity test of the compounds on the cell line using MTS assay
- 4. Examine antiviral activity of the selected compounds by immunoperoxidase assays (IPMA) and quantitative Real-time PCR

Materials and Methods

Objective 1: To screen the candidate small-molecular compounds from available and purchasable databases that bind to 3CL^{pro} of FCoV specifically and with high affinity by the computer aided screening

Specific work:

1) Retrieve crystal structures of FIPV 3CL^{pro} from PDB databases and prepare the structures for virtual screening

Crystal structure of main protease (M^{pro}), is also known as the 3C-like protease (3CL^{pro}), were obtained from the Protein Data Bank (PDB) (ID: 5EU8 and 4ZR0, respectively).

2) Process the simulation structure by removing sulfate ion and water and adding H-bond

The files were prepared for further molecular docking analysis by removing all sulfate ions and water molecules. Process the simulation structure by removing sulfate ion and water and adding H-bond were performed. The PDB file was prepared for further molecular docking analysis. The structure was processed to prepare for the molecular docking studies. Briefly, the preparation consisted of adding hydrogen atoms, eliminating water molecules, removing some ions, specifying the correct protonation and tautomerization states of the binding site residues, and calculating partial charges using Chimera (UCSF, USA) as the recommendation by Jain and Nicholls 2008. The prepared structure was saved (pdb and mol2 files) for further molecular docking analysis.

- 3) Set up the libraries of chemical compounds from databases
 - 3.1) Setting up the initial libraries of chemical compounds from databases

Available compound libraries include ZINC (UCSF), Pubchem, NCI, PDB ligands and ChEMBL databases were acquired to generate initial compound libraries for the screening process (Table 1).

Table 1. Available compounds from each database to set the initial libraries

Compound library databases	Numbers of retrieved compounds	
1. ZINC	999,970	
2. Pubchem	1,382,146	
3. NCI (diversity and natural)	5,336	
4. PDB ligands	1,096	
5. Other: ChEMBL, drug bank	1,200	
Total compounds	2,389,748 compounds	

3.2) Retrieved initial ZINC compounds from ZINC database by using Idock screening server

A set of compounds to dock using Idock server (http://istar.cse.cuhk.edu.hk/idock/) was performed. Totally, 23,129,083 compounds were collected from ZINC database. Compounds satisfying all the 9 filtering conditions was docked including molecular weight (g/mol), partition coefficient xlogP, rotatable bonds, hydrogen bond donors, hydrogen bond acceptors, net charge, apolar desolvation (kcal/mol), polar desolvation (kcal/mol) and polar surface area tPSA (\mathring{A}^2). The input to Idock includes a rigid receptor, a set of flexible ligands, and a cubic box, which is used to restrict the conformational space to a particular binding site of the receptor. The cubic size was consisted of grid center (x = -40, y = -10, z = -5) and size (x = 30, y = 40, z = 25), respectively. The range of molecular weight was 101–500, H-bond 2–4 bonds, log P (1,3) and H-acceptor 4–7 atoms, respectively. The number of compounds satisfying all the 9 filtering conditions was 999,970 compounds. The best-predicted conformations of the top 1000 hit compounds were performed. The output from Idock server included the predicted conformations and their predicted binding affinities. The results were collected and would be performed for further docking.

3.4) Retrieval initial compounds form NCI, Pubchem and ChEMBL databases

The natural and synthetic compounds were retrieved from these databases. The compounds structures of ligands are saved in mol2 format for docking calculations, and in Structure Data Format (i.e., SDF format by MDL Information Systems) format for 3-D applications like docking, For 2-D methods like scaffold hopping, it was also stored as SMILES format. The total compounds used for the 1st filtering were shown in Table 1.

The selected compounds from each databases were created to be small and separated libraries so that each library contained less than 500 compounds (up to 100 separated libraries)

Then, the selected compounds were screened (the 1st filtering), and the selected compounds were saved for further molecular docking. The compounds were filtered and based on drug-like or lead-like physiochemical properties (Table 2)(e.g., Lipinski's rule of five [Lipinski, et al. 1997], and lead-like filters suggested by Oprea et al, 2002.

Table 2. The typical properties used for lead-likeness and drug-likeness criteria

Properties	Lead-likeness	Drug-likeness
Molecular weight (MW)	≤ 300-350	≤ 500
Lipophilicity (clog P)	≤ 3.0	≤ 5.0
H-bond donor (sum of NH and OH)	≤ 3	≤ 5
H-bond acceptor (sum of N and O)	≤ 8	≤ 10
Polar surface area (PSA)	≤ 120 Ų	≤ 150 Ų
Number of rotatable bonds Structural	≤ 8	≤ 10
filters	≤ 22	
Heavy atom	Reactive groups	
	Warhead-containing	
	agents Frequent hitters	
	Promiscuous inhibitors	

- 4) Dock the ligand onto the structural file and visualize using molecular software, and
- 5) Calculate the force fields between the interacting complex using computer software

5.1) Molecular docking of protein-ligands

The ADMET (Absorption, Distribution, Metabolism, Elimination and Toxicity) analysis was subsequently performed on the selected compounds using DataWarrior version 4.1.1 [Sander et al., 2015] as the 2nd filtering. Three molecular docking programs were used to perform structural preparation, selection and evaluation of the initial compounds with the best binding energy as the 3rd filtering.

5.2) Autodock Vina

The initial mentioned compounds in Table 3 were performed using AutoDock Vina version 4.1.1.2 [Morris et al, 2009] by PyRx suite open-source software version 0.9.4 that is a new knowledge-based empirical scoring function of ligand-protein complex [Dallakyan S and Olson AJ. 2015]. The input files used for virtual screening were converted to the pdbqt file format for docking with AutoDock Vina. The grid center and dimensions were consisted of grid center (x = -40, y = -10, z = -5) and size (x = 30, y = 40, z = 25), respectively. Lamarckian Generic Algorithm (GA) was used for the docking. This GA parameters set by default included; 10 GA runs, 150 individual in population, 270,000 maximum numbers of energy evaluation and 0.02 gene mutation rate and 0.8 cross over rate. The outputs of the ten best binding poses for each docking run were stored. These molecular docking programs selected the best-ranked compounds from all libraries with the ranked binding energy less than the cut-off of -7.0 kcal/mole

5.3 GOLD

GOLD v5.5 is based on a genetic algorithm [Jones et al, 1997]. Intuitive protein-ligand docking package license was kindly provided by Assoc Prof Dr Kiattawee Choowongkomon, Faculty of Science, Kasetsart University. The grid box was centered at the interface region similar to that set for PyRx. This GA parameters set by 30 GA runs. Score function was ChemScore fitness function, which incorporates a protein-ligand atom clash term and an internal energy term. ChemScore takes account of hydrophobic-hydrophobic contact area, hydrogen bonding, ligand flexibility and metal interaction.

5.4 ICM

ICM v3.8-6 (Full-package, 30-Day trial license) calculates energy based on the Empirical Conformational Energy Program [Abagyan et al, 1994]. A global optimization procedure is used to undertake an unbiased, all-atom, flexible docking of the ligand within the rigid binding pocket using PocketFinder. This procedure consists of the following steps: (1) a random conformational change of the free variables according to the biased probability Monte Carlo (BPMC) algorithm), torsion and rotational angles of the ligand, (2) local energy minimization of the analytical differentiable terms, (3) calculation of the complete energy, including non-differentiable terms, (4) acceptance or rejection of the total energy on the basis of the Metropolis criterion and (5) allocation of favorable conformations to a conformational stack that both expels from unwanted minima and promotes the discovery of new minima. The thoroughness or effort value was 10 for each

docking job. The grid size and grid center were adjusted similar to that set for the twomentioned software.

5.5 Consensus scoring

The combining ranks from three individual scoring functions were performed to improve enrichment. Combining predictions from different models to generate a consensus. In practical virtual screening, it is common practice to select a top portion of a library of ranked compounds for further evaluation, but the size of such portions is somewhat arbitrary and, clearly, extremely dependent upon the initial library size [Chen et al, 2006]. The evaluated consensus scoring methods and their performances were used the "rank-by-rank" strategy in the consensus scoring to combine the results of multiple scoring functions [Wang and Wang, 2001] was suitable because the scoring functions give results were not in a compatible unit. The best accuracy and enrichment was obtained from Autodock Vina (PyRx), Chemscore of GOLD and ICM scores.

5.6) Predicted xenobiotic metabolism

The best-ranked compounds were subsequently analyzed to identify the predicted sites for xenobiotic metabolism using MetaPrint2D, a free online software (http://www-metaprint2d.ch.cam.ac.uk/metaprint2d), which predicts sites of phase I metabolism, defined as the addition of oxygen (e.g. hydroxylation, oxidation, epoxidation) or elimination reactions. The illustrations were demonstrated with different colors for the predicted sites of each compound. The color schemes of the predicted metabolic site are red (0.66–1.00), orange (0.33–0.66), green (0.15–0.33), white (0.00–0.15) and grey (little), respectively. In case of the MetaPrint2D is not available (at this time of final TRF report). The XenoSite Metabolism and Reactivity Prediction Web Server from The Washington University in St. Louis, School of Medicine were performed for metabolism prediction of the ligands (http://swami.wustl.edu/xenosite/).

5.7) Characterization of the interactions of protein-ligand complexes

The protein–ligand complexes obtained from the docking results were evaluated on how the compounds or ligands interact with their protein targets. The protein–ligand interaction profiler (PLIP version 1.3.4), freely available at projects.biotec.tu-dresden.de/plip-web, was used to detect and visualize the binding between molecules of non-covalent interactions of protein–ligand complexes such as hydrophobic interactions, hydrogen bonds, salt bridges and π -stacking. The result files from the docking software were uploaded to the server as the input data. The output results were saved as 2D and

3D interaction diagrams and then exported for visualization by PyMOL version 1.7.4.5 (www.pymol.org).

Objective 2: To evaluate the candidate compounds for their inhibitory activity against FIPV replication *in vitro* using cell-based assay.

Specific work:

1) Additional plans were performed in vitro as followed;

Objective of the additional plan: The aim of this study is to test the candidate antiviral lead compounds that can inhibit FIPV protease activity and FIPV3CL^{pro}.

1.1) Construction of recombinant FIPV 3CL protease

The coding sequence for FIPV main protease (FIP3CL^{pro}) was amplified from FIPV strain 79-1146 and subcloned into the vector pGEM Easy (Promega, Co., Madison, WI, USA) at Kasetsart University, Thailand. Then, the gene encoding FIPV main protease were amplified with primers (forward, 5'-CAT GCC ATG GCT ATC GAG GGA AGG TCC GGA TTG AGA AAA ATG GCA C-3'; and reverse, (5'-CCG CTC GAG TTA CTG AAG ATT AAC ACC ATA CAT TTG C- 3') containing NCol and Xhol restriction sites (underlined). The PCR product was digested by NCoI and XhoI by using NCoI and XhoI restriction enzymes, and then ligated into pET32a vector, which contains a Thioredoxintag (Trx-tag) and His-tag at N-terminus [Kuo et al, 2004]. The recombinant protease plasmid was used to transform Escherichia coli (E.coli) strain DH50 competent cells (ECOS 101, Yeastern Biotech Co., Ltd, Taiwan). The competent cells were streaked on a Luria-Bertani (LB) agar plate containing 100 μg/ml ampicillin. Ampicilin-resistant colonies were selected from the agar plate and then grown in 5 ml LB culture containing 100 μg/ml ampicillin at 37°C overnight. The recombinant plasmid was verified by sequencing and the correct construct was subsequently transformed into E.coil strain BL21 (DE3) for protein expression. A single transformant was grown in 5 ml LB medium as described above before transferring to 500 ml of fresh LB medium containing 100 µg/ml ampicillin. Transformants were cultured until the optical density at 600 nm reached 0.6, and then the cultures were induced by 0.5 mM isopropyl- β -thiogalactopyranoside (IPTG) to express FIP3CL^{pro} at 16°C overnight.

The *E.coli* were harvested by centrifugation at 6,000 rpm for 15 min. The cell pellet was obtained from 2-L cell culture was suspended in 20 ml cold PBS buffer. The protein purification was performed at 4°C by mechanically disruption at 12,000 psi and then the lysis solution was chemically digested using 1 mg/ml lysozyme HCI (GERBU,

Biotechnik Bmbh, Germany) at 4°C for 30 min. The lysis solution was centrifuged at 14,000 rpm, and the debris was discard. The clear, cell-free solution of the protein (20 ml) was loaded to a Ni-NTA column. The column was washed with cold PBS and 5 mM imidazole followed by 30 mM imidazole-containing PBS buffer. The Trx- and His-tagged FIP3CL^{pro} was eluted with 300 mM imidazole-containing PBS buffer. Protein purity was increase by repeating the purification process and the imidazole were removed by exchanging the buffer to cold PBS buffer (pH 7.0). Ten microliters of Factor Xa protease (1mg/ml) (New England BioLabs Inc., USA) was used in order to remove the tags, and the mixture was loaded onto the Ni-NTA column. The untagged FIP3CL protease in the flow-through was subsequently dialyzed in dithiothretol (DTT) buffer (12mM Tris-HCl, 120mM NaCl, 0.1 mM EDTA, 1mM DTT) for storage. The purified proteins were concentrated and the purity was determined by SDS-PAGE analysis. The protein with purity more than 90% was subjected to the next experiment.

1.2) Determining FIP3CL^{pro} activity

The enzyme kinetics is a study on enzyme-catalytic reactions by measuring on enzyme-substrate reaction by time. This study included the measuring rates of the enzyme-catalytic reactions at different substrate concentrations. The fluorogenic peptides (Dabcyl-KTSAVLQSGFRKME-Edans) used for testing, as protease substrates, were kindly provided by Asst. Prof. Dr. Chih-Jung Kuo (Figure 1). The substrate specificity of the protease was performed using the fluorogenic peptide as previously reported [Kuo et al, 2004]. The protease enzyme kinetic measurements was implemented after incubating 6 μ M fluorogenic peptide with 35 nM protease in 20 mM Bis-Tris buffer (pH 7.0, the optimal pH for protease activity), and different concentrations of the fluorogenic substrate (0.5, 1, 2, 5, 10, and 20 μ M) at 25°C for 20 min. The enhanced fluorescence due to cleavage of the peptide was monitored at 538 nm (Dabcyl) with excitation at 355 nm (Edans) using a fluorescence plate reader (BMG FLUOstar OPTIMA Microplate Reader, UK). The initial rate within 10% substrate consumption was used to calculate the kinetic parameters using Michaelis—Menten equation fitting by the KaleidaGraph computer program (PA, USA) [Kuo et al, 2004].

Figure 1. The fluorogenic substrate used for FIP3CL protease inhibition assay in this study [Wu et al, 2004]

To determine the FIP3CL protease kinetics, the rate of catalysis (also known as the reaction velocity) vs. the fluorogenic substrate concentration [S] at the fixed enzyme concentration (35 nM FIP3CL^{pro}) was plotted. The velocity (V) varied linearly with [S] for low amount of [S] as the initial rate. As [S] increases, V "plateaus" indicating that V becomes independent of [S] at high amount of [S]. The model of enzyme reaction is an equation (1)

$$\begin{array}{ccc}
k_1 & k_2 \\
E + S \leftrightarrow ES \rightarrow E + P \\
k_{-1} & & \\
\end{array}$$
(1)

E is the enzyme. S is the substrate. ES is the enzyme-substrate complex. P is the product of the enzyme-catalyztic reaction. k1 is the rate constant of the forward reaction of E+S. k₋₁ is the rate of the reverse reaction where the enzyme-substrate complex, ES, falls apart to E+S and k2 is the rate constant of the forward reaction of ES forming E+P. Under the steady-state approximation, the concentration of the intermediate [ES] should stay a constant, while the concentrations of reactants and products can change. The equation is rearranged the steady-state as shown in equation (2)

$$k1 [E] [S] = (k-1 + k2) [ES]$$
 (2)

Then substitution of K to Km, the Michaelis constant, as shown in the equation (3)

$$[ES] = [E][S]/Km \tag{3}$$

The maximum reaction velocity, Vmax, is reached when all enzyme sites are saturated with the substrate. This happens when [S] is less than Km, so that [S]/([S]+Km)

approaches and V could be expressed by multiplied by [S]/([S]+Km) Vmax as shown by Michaelis-Menten equation (4)

$$V = V_{\text{max}} \frac{[S]}{[S] + K_{M}}$$
(4)

From all simplified equations above, Km is equal to the substrate concentration at which the reaction rate is half its maximum value or at which velocity (V) is exactly 1/2 of Vmax. In other words, if an enzyme has a small value of Km, it achieves its maximum catalytic efficiency at low substrate concentrations. So, the smaller the value of Km, the more efficient is the catalyst. From the equation (1), The Kcat, the turnover number, is k2 in the specific Michaelis-Menten kinetic mechanism as equation (4) above. Kcat relates Vmax to enzyme [E] in the total active site concentration. The Kcat/Km ratio is the criterion of substrate specificity and catalytic efficiency. The higher the Kcat/Km, the better the enzyme works on that substrate

1.3) Determination of FIP3CL^{pro} inhibition activity

Enzyme inhibition assay was performed on the selected compounds (20 compounds) selected by *in sillico* analysis in Thailand. To measure the inhibition constant measurements of FIP3CL pro, the reactions were performed with 35 nM FIP3CL pro in the 20 mM Bis-Tris buffer mixture. Compounds were dissolved in DMSO to 10 mM to assay for inhibition test. The fluorescence changes resulting from the reaction between the enzyme and substrate was read and recorded by a 96-well fluorescence plate reader. To determine the inhibitory effects of the compounds, the different concentrations of 100, 50, 25, 10, 5, 2.5, 1, 0.5 μ M of each compound and the enzyme mixture were pre-incubated for 10 min prior to the addition of 6 μ M fluorogenic substrate and the fluorescent change was evaluated as mentioned above. The fluorescence changes obtained time from each compound was plotted. The calculated slopes from each concentration of each inhibitor were then compared those to the slope of control well (DMSO) within the same running. The average slope of the control wells was assumed as 100%. The relative reduction of enzyme activity of each compound was calculated to obtain a half of inhibitory concentration (IC50) using GraphPad Prism 5.0 (Prism, CA, USA).

2) Development of cell-based assay for FIPV3CL protease analysis (as mentioned contract)

2.1) Viral propagation and titration

2.1.1) Cell culture and virus

Crandell-Rees feline kidney (CRFK) cell line (ATCC, CCL-94) was used for virus propagation and titration. The cell lines were maintained in Modified Eagle Medium (MEM, Invitrogen, CA, USA), supplemented with 7% fetal bovine serum (FBS, Invitrogen, CA, USA), 2 mM L-glutamine (Invitrogen, CA, USA) and antibiotics-antimycotics (Invitrogen, CA, USA). CRFK cell lines were seeded at 1 x 10⁶ cells/ml in a 6-well plate and incubated at 37°C, with 5% CO₂. At 24 hour post seeding, the cells would be 70-80% confluent. FIPV strain 79-1146 strain (ATCC, USA) was inoculated onto an overnight grown CRFK cells at ratio 1:5, and incubated at 37°C with CO₂ for 48 hours. The development of cytopathic effect (CPE) was observed by an inverted microscope.

For virus propagation, the infected cells and virus-containing supernatant were then subjected to a double freeze/thaw cycle to release cell-bound viruses, and the samples were clarified by centrifugation at 2000xg at 4°C for 10 min. The viruses were passaged in the CRFK cells for 5 passages. The FIPV infected CRFK cells form each passage was kept at -80°C for virus detection and quantification.

2.1.2) Viral titration

The 5th passage of FIPV strain 79-1146 was 10-fold serially diluted from 10^{-1} , 10^{-2} , 10^{-3} , 10^{-4} , 10^{-5} , 10^{-6} to 10^{-7} with MEM. The CRFK cells were grown in a 96 well-plate and inoculated with the various dilutions of FIPV for 2 hr to allow viral adsorption at 37° C. Then, the media was added to the final volume of 100 μ l. The cells were observed for the development of cytopathic effect (CPE) everyday.

2.2) The Immunoperoxidase Monolayer Assay (IPMA) for the detection of FIPV strain 79-1146

The CRFK cells were grown onto 96-well for 24 hrs, and viruses from each passage were inoculated onto the CRFK cells for 24-48 hour post infection (hpi). The cells were fixed with cold methanol at room temperature for 20 min, and then washed with PBST buffer. The primary antibody for FIPV detection, a mouse monoclonal antibody specific to pan-coronavirus FIPV3-70 (dilution 1:500, ThermoFisher, USA), was incubated with the infected cells at 37°C for 1 hour. After washing using PBST, the secondary antibody, a goat anti-mouse IgG-HRP antibody (dilution 1:400, KPN, USA), was incubated at 37°C for 1 hour. Antigen and antibody reaction was stained by using DAB substrate

(DAKO, Germany), and the reaction was observed under a phase contrast inverted microscopy.

2.3) Determination of optimal cells and virus concentration

In order to obtain the optimal condition for cell-base FIPV 3CL protease inhibitory assay, an experiment was performed to determine the viral dose and CRFK cell concentration. The CRFK cells were seeded with different concentrations – $1x10^5$ cells/ml (100 μ l/well) and $5x10^5$ cells/ml (100 μ l/well) – onto a 96-well plate. The cells were incubated at 37° C for 24 hours. The viruses were inoculated at the doses of 1000 TCID₅₀ and 100 TCID₅₀ per well. The three biological replications were performed for each condition. The CPE was observed every day. The cell viability in each treatment well was examined and compared with the mock cells at 24 and 48 hour post inoculation (hpi).

The percentage of viable cells was detected using MTS assay using the Cell-Titer 96 non-Radioactive Cell Proliferation Assay Kits (Promega Co., Madison, WI, USA) to determine the population of living cells. Twenty microliters of MTS/PMS (Promega Co., Madison, WI, USA) were added into each well and mixed gently. The plate was incubated at 37°C with 5%CO₂. After MTS/PMS incubation at 37°C for 2 hours, the absorbance of the samples was measured with a plate reader at 490 nm. The OD value from the wells were subtracted by the absorbance of the blank wells (CRFK cell with MEM), and then the absorbance of the virus infected wells, which contained the cells with virus, was divided by the average of the absorbance emitted from the control wells.

2.4) Cell-based assay for the candidate compounds

2.4.1) Cytotoxicity assay

The CRFK cells were seeded at 1×10^5 cells/ml (100 μ l/well) onto 96-well plate and incubated overnight. After the incubations with the tested compounds at varied concentrations (200, 100, 10, 1 and 0.1 μ M) for 48 hours, the culture medium was added with 20 μ l of MTS/PMS per well. After MTS/PMS incubation at 37°C for 2 hours, the optical density of the each sample was measured with a plate reader at 490 nm. The sample wells were subtracted by those of the blank wells. The absorbance of the compound treatment wells was divided by the average of the absorbance of the control wells. The ratio of inhibition was calculated. Data was expressed as percentage of OD from compound treatment wells relative to OD of the control cells (as 100%) cultured in the absence of any tested compounds [Shie et al, 2005].

2.4.2) Antiviral activity assay

Antiviral activities of the candidate compounds were examined using CRFK cells infected with different concentrations of FIPV for 24 hrs by following three conditions:

2.4.2.1) Pre-viral entry activity

In order to determine if the compounds could inhibit FIP3CL^{pro} activity at the time before virus entry to the host cells, the CRFK cells were seed at $5x10^4$ cells/well onto 24-well plate and incubated overnight as mentioned above. The FIPV strain 79-1146 at 100 TCID₅₀ was inoculated into each well in the presence or absence of different compound concentrations. The compounds were added to final concentrations at 0.5, 1.0, 5, 10, 20, 50 and 100 μ M per well depending on the CC₅₀ values from the cytotoxicity assay. The cells were incubated at 37°C for 24 hrs. The antiviral activity was determined by the presenting of FIPV antigens using IPMA as described above and the viral quantification using real-time qPCR.

2.4.2.2) Post-viral entry activity

In order to determine if the antiviral activities of the candidate compounds against intracellular replication of FIPV, the CRFK cells were inoculated with FIPV at 100 $TCID_{50}$ /well. The infected cells were incubated at 37°C for 2 hrs for viral adsorption. Then, the infected-CRFK cells were incubated with the different concentrations of each compounds for 24 hours. Antiviral activity was evaluated by the reducing of FIPV-infected cells and antigens using IPMA and viral nucleic acid by RT-qPCR.

2.4.2.3) Prophylaxis activity

In order to determine if the candidate compounds could enter into the host cells and had antiviral activity after FIPV infection. The CRFK cells were seed at $5x10^4$ cells/well into 24-well plate and incubated overnight. The different concentration of compounds were added into each well and the cells were incubated at 37° C for 2 hrs before washing once with the ringer's saline solution (pH 7.4). The FIPV at 100 TCID₅₀/well was inoculated into each well and the cells were incubated at 37° C for 24 hrs. Antiviral activity was evaluated by the presenting of FIPV infected cells and antigens using IPMA and viral nucleic acid by RT-qPCR.

2.4.3) Image analysis

Antiviral activities of the tested compounds were evaluated by measuring the intensity and the numbers of the positive FIPV-infected CRFK cells using IPMA assay. Five concentrations of each compound were added to 96-well plates in triplicate to obtain the effective concentration.

For EC₅₀ evaluation of antiviral activity, Image analysis of the presenting of FIPV antigens in the infected cells was performed using the CellProfiler software (2.7.0) with open-source code of available algorithms (Broad Institute; freeware available at http://www.cellprofiler.org/ index.htm). The five images from each concentration of the tested compounds were used for the analysis. CellProfiler pipeline utilized in this project was modified from the open-source in GitHub (https://forum.image.sc/t/relate-dab-staining-to-nuclei/12361). The pipeline, IPMA1.cppippe, was developed to calculate the intensity of the DAB stained cell parts compared to the unstained cell parts, and set to distinguish clumped objects compared to the shape of the objects.

All three conditions, the effectively antiviral concentrations of those compounds were determined as the active compound concentration that inhibited FIPV infection to host cells by 50% of the control value (EC_{50} or 50% effective concentration). The raw data from image analysis were converted to log_{10} transform data for calculating EC_{50} values, which the percent of FIPV inhibition was define as the logarithmic interpolation of the following four parameters:

A: compound concentration at which % antiviral activity is less than 50%

B: compound concentration at which % antiviral activity is more than 50%

C: value of % antiviral activity more than 50%

D: value of % antiviral activity less than 50%

Which these were calculated the EC₅₀ using the following equation of;

$$EC_{50}$$
 value = $10^{((Log(A) - Log(B)) \times ((C-50)/(C-D)) = Log(B))}$

The concentration of compound at which the presenting of positive FIPV infected cells is reduced by 50%. An active compound or "hit" is any compound that exhibited a % FIPV-positive cell inhibition of more than 50% without compromising cell viability. The

effective concentration at which the compound inhibited 50% the infected- positive cells (EC_{50}) or in the absence of virus as mentioned above was determined. The selective index (SI) was calculated as SI = IC_{50}/EC_{50} .

2.4.4) Examination of compound inhibition activity on the FIPV-infected CRFK cells by quantitative real-time PCR.

In order to quantify the total amount of FIPV after compound inhibition, the compound number 1, 3, 4, 5, 13 and drug controls (ribavirin and lopinavir) for the three anitiviral activities were performed.

2.4.4.1) RNA extraction and cDNA synthesis

The supernatant will be collected at specific times post infection for the detection of viral nucleic acids. Viral RNAs were extracted using Trizol Total RNA extraction protocol according to the manufacturer (Invitrogen, USA). The RNA yield and purity was determined by spectrophotometry (OD 280/260) Nanodrop 2000 (Thermo, CA, USA). The purified RNA was used as the templates for cDNA synthesis using Superscript III (Invitrogen, CA, USA) following the manufacturer's protocol. The RNA was denatured at 70 °C for 10 min. The cDNAs were synthesized at 42°C for 50 min followed by incubation at 70 °C for 15 min. All cDNA samples were then stored at -80 °C until used.

2.4.4.2) Sequencing of qPCR amplicon

Two FIPV specific primers were used for the nucleic acid quantification. The primers for FIPV PCR targets to the 3'-untranslated region (3'-UTR) of ORF6b was used [Herrewegh et al, 1995; Manasateinkij et al, 2009]. The sequences of the primers specific to FCoV viral genome are 5'-GGCAACCCGATGTTTAAAACTGG-3' (upstream; nucleotides 1 to 23) and 5'-CACTAGATCCAGACGTTAGCTC-3' (downstream; nucleotides 211 to 192). The PCR amplication were amplified using Taq DNA polymerase (Invitrogen, USA) in a 10 μ l reaction containing 1 μ l cDNA, 10 μ M forward primer, 10 μ M reverse primer, 10 mM dNTP, 5 units of DNA polymerase, 1× PCR buffer and 25 mM MgCl₂. The reactions were initial denaturation at 94°C for 3 min followed by 35 cycles of 94°C for 30 sec, 52°C for 30 s and 72°C for 20 sec and the final incubation at 72°C for 7 min, the DNA was stored at 4°C. The PCR product was visualized by using 1% of agarose gel.

The PCR products were purified using HiYieldTM Gel/PCR Fragments Extraction Kit (RBC Bioscience Corp., USA). The 3'-UTR sequence of FIP amplicone was inserted

to the pGEM T-easy plasmid vector (Promega, USA). Plasmids were then isolated using QIAprep Spin Miniprep Kit (Qiagen). The inserts were sequenced using T7 sequencing primers (5´- TAATACGACTCACTATAGGG- 3´).

2.4.4.3) Quantitative real time PCR assay

Quantitative amplification and melting curve analysis will be carried out by the real-time quantitative PCR (qPCR) (C1000 Touch Thermal Cycler, Bio-Rad, USA). The total qPCR reaction volume of 10 μ l contained 5 μ l using SsoFast EvaGreen Supermix (2x) (Bio-Rad, USA), 4 μ l template cDNA and 0.5 μ l. The primer set was mentioned in 2.4.4.2 used for detection. The cycling condition are as follows: initial denaturation of DNA at 95°C for 30 sec, 30 cycles of 5 sec at 95 °C of denaturation, 5 sec at 60 °C of annealing and extension, and followed by a melting curve analysis from 65–95 °C with 0.5°C increment. The qPCR were carried out of the two biological and two technical replications.

2.4.4.4) Plasmid copy number determination

Plasmid contained FIP 3'-UTR sequence was ten-fold serially diluted from 10⁻² to 10⁻⁷ to generate a standard curve. This set of 6 dilution plasmids was included in each run. For real-time PCR analysis, the threshold was manually place on at 10² relative fluorescence units (RFU). The standard curve was generated using a linear part of the amplification curves plotted against the log values of the starting concentrations that r² ≥ 0.99. The slope of the standard curve was used to calculate amplification efficiency (E) expressed in percent of 90–100%. The Cq values were then automatically generated by CFX Maestro™ software (Biorad, USA). The absolute quantification of viral copy numbers of each experiment was calculated by individual experiment.

All statistical analyses of genome copy numbers from the FIPV-infected CRFK cells treated with the varied concentration of the compounds were compared to those from viral control using GraphPad Prism version 5.0 (GraphPad, CA, USA). A p-value of less than 0.05 was considered as statistically siginificance. The dose-response curves of the antiviral activity represent candidate compounds were plotted.

3) Molecular dynamic simulation

Molecular dynamic simulation was performed in order to investigate the structure and dynamic behaviors of the FIP3CL^{pro} and its ligsnds that showedwith the best results from the cell-based assay.

3.1) Protein and ligand structure preparation

The ligand–protein interactions were performed using free protein (free FIP3CL^{pro}) complexed with the compound 1 (FIP3CL^{pro}–cpd 1 complex). The X-ray structure of the FIP3CL^{pro} (PDB code: 5EU8; 2.447 A° resolution) was used as the template model to construct the FIP3CL^{pro}–cpd1 complex. The initial complex model obtained from the docking results was prepared prior to simulation by rationalizing the model conformation using AMBER 12 software package (kindly provided by Dr. Sissades Tongsima, Head of Biostatistics and Informatics Laboratory, Genome Institute, BIOTEC, Thailand).

3.2) Energy minimization and Molecular Dynamic (MD) Simulations

Energy minimization and MD simulations were carried out using the SANDER module of AMBER 12. First, the Cartesian coordinate preparation directly provided the force fields for proteins and nucleic acids as well as water models and other organic solvents in FIP3CL^{pro}–cpd1 complex structure. To generate coordination, the complex conformations contained a phosphate group and cysteine and histidine residues were changed in an editor script from CYS to CYX and HIS to HID. Second, the parameters of force field selection and the topology files were generated using tleaf module. Finally, the energy minimization and dynamics of parameters were subsequently performed following the steps of equilibration, production of molecular dynamics (MD) runs, and analyses of trajectories. The minimization was carried out to relax all systems prior to performing the MD runs. Hydrogen atoms, ions, and water molecules were minimized to restrain the total energy in 10,000 steps using the steepest descent method to under 0-5 kcal/mol. The production run phases of MD using the system temperature was gradually raised from 0 to 300 K for the first 600 picosecond (ps) and then kept constant with the time step of 0.002 ps, and the final step of running from 200 ps to 6 ns. The average of the trajectories production phase were calculated and the all MD simulation were performed for 25 nanosecond. The MD trajectories were evaluated in terms of root-mean-square displacement (RMSD) using the cpptraj module of AMBER 12 package. The visualization of RMSD of .rms file was analyzed using Xmgrace software (Version 5.1.19, Turner, 2005). The distances and H-bonds were determined using the PLIP software (https://projects.biotec.tu-dresden.de/plip-web/plip/index) (Salentin et al, 2015)

Results

Objective 1: To screen the candidate small-molecular compounds from available and purchasable databases that bind to 3CL^{pro} of FCoV specifically and with high affinity by the computer aided screening

Both structures of FIP main protease contain 3 domains. Domains I and II are appeared as antiparallel β -barrels, and domain III contains five alpha-helices. The binding pocket is located between domain I and domain II and composed of cysteine residue (CYS 144). Evaluating superposition across all 299 fully populated columns in the final alignment:

- RMSD of 4zro.pdb, chain A with 5EU8, chain A: 0.966

- Overall RMSD: 0.966

- Sequence lengths: 1-299

- SDM (cutoff 5.0): 19.189

- Q-score: 0.903

- RMSD between 299 atom pairs is 0.964 angstroms

The matched 5EU8 5EU8, chain A to 4zro.pdb 4zro.pdb, chain A with 0.964 RMSD (299 atom pairs) was similarity as shown below;

- 4zro.pdb, chain A vs. 4zro.pdb, chain A: 100.00% identity
- 4zro.pdb, chain A vs. 5EU8, chain A: 100.00% identity
- 5EU8, chain A vs. 4zro.pdb, chain A: 100.00% identity
- 5EU8, chain A vs. 5EU8, chain A: 100.00% identity



Figure 2. The superimposed structure of 5EU8 (blue) and 4zro (orange) pdb files

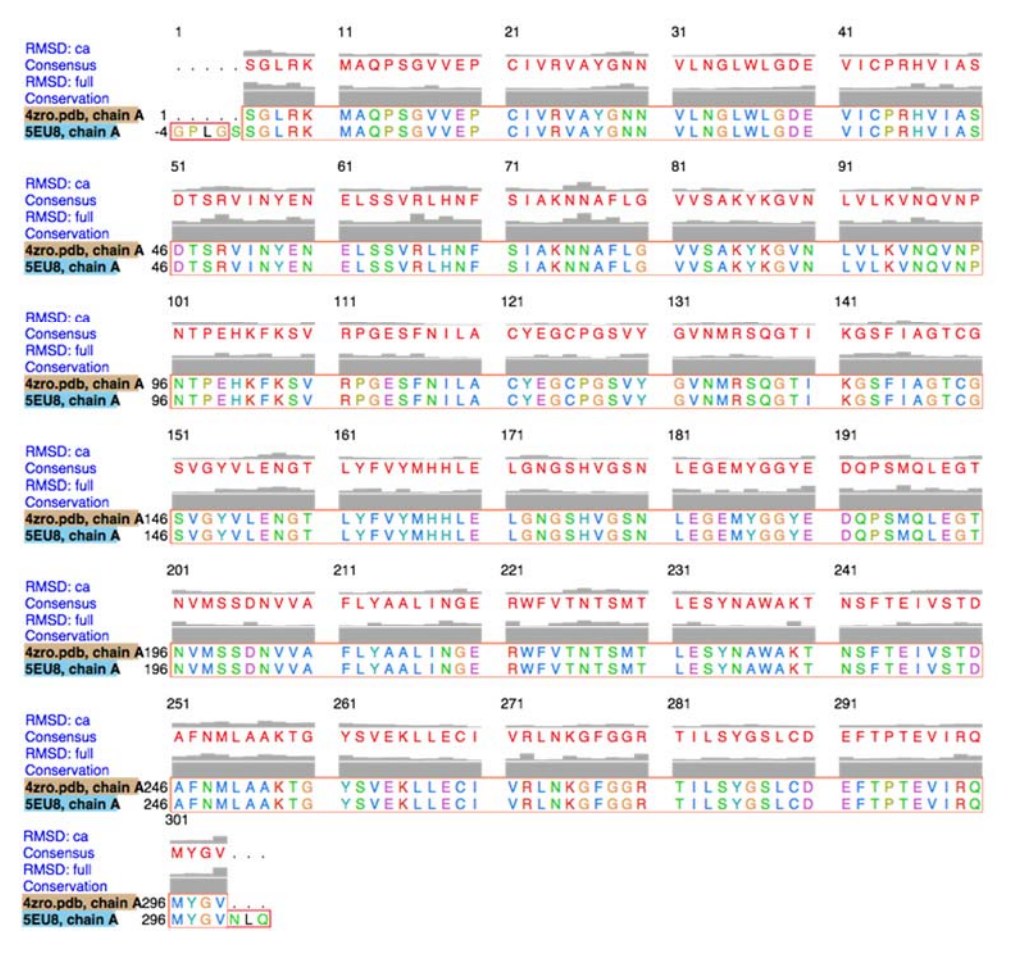


Figure 3. Structure-based sequence alignment of two sequences and details of RMSD, consensus and conservation

The retrieval initial compounds form the available databases were performed by filtering. The total of the 1st filtered compounds was approximately 678,612 compounds (Table 3). The second filtering were filtered and based on the drug-like or the lead-like physiochemical properties. The 2nd filtered compounds were approximately 2,764 compounds for further molecular docking analysis.

Molecular docking analyses among three software were carried out using the Autodock Vina, Gold and ICM software. The best hit of the candidate compounds were ranged by the best affinity binding, and then were used the consensus analysis to narrow down their hits. The best AUC value observed among the consensus scoring methods was comparable to the best AUC observed for the individual scoring functions. Our validation dataset consisted of 86 compounds was sufficient to perform. The results showed a significantly higher AUC (= 0.827, range from 0.742–0.849) than the combination of two scoring functions (Figure 4). However, the corresponding

combinations of individual scoring functions of Autodock Vina (PyRx) and ChemScore was slightly higher than the three combination programs.

Table 3. The total number of initial compounds from different libraries that followed the Linpinski's rule of five

	Type of compounds	Number of	Lipinski's rule of 5 and
		compounds	purchasable compounds
1	ZINC compounds	643,628	1,000 top rank
2	NCI diversity set III	1,597	100 top rank
3	NCI diversity set IV	1,596	100 top rank
4	NCI diversity set V	1,593	100 top rank
5	NCI natural product II	120	50 top rank
6	NCI natural product III	117	50 top rank
7	NCI natural product IV	419	100 top rank
8	Peptide-like compound	72	72
	(PDB database)		
9	Amentoflavone	10	10
10	Apeginin	15	5
11	Balcalein	25	14
12	Baicalin	8	-
13	Biflavavone	21	10
14	Biflavone	49	12
15	EGCG	13	-
16	Fisetin	14	14
17	Flavone	1,000	200
18	Glabranine	1	1
19	GCG	6	-
20	Hyperoxide	3	3
21	Ladanein	1	1
22	Luteolin	235	14
23	Quercetin	200	134

24	Ajoene	3	2
25	Allicin	4	3
26	Andrographolic	29	9
27	Caffeic	88	18
28	Cavacal	44	18
29	Catechin	149	8
30	Cinnamaldehyde	256	32
31	Coumarin	2,129	373
32	Curcumin	78	20
33	Decahydroisoquinoline	1,807	20
34	Etacrynic	2	1
35	Eugenol	57	33
36	Flavonoid	8	8
37	Genistein (isoflavone)	25	15
38	Isatin	499	150
39	Menthol	118	9
40	Pyrimidine	380	18
41	Rosmarinic acid	7	2
42	Steviol	15	8
43	Terpenoid	8	-
44	Anthocyanin	2	1
45	Kaempferol	527	12
46	Piperine	6	3
47	Theaflavin	21	-
48	Tinosporon	1	-
49	Ursolic acid	1	-
50	Triterpenoid	7	-
51	Rutin	31	1
52	Cucurbitane	3	-
53	Cucubitine	2	3

Total	678,945	2,764	
1.2- 1.0- 1.0- 0.8- 0.6- 0.4- 0.2-	— Pyrx+Chemscore+I — Pyrx+Chemscore, A — Pyrx+ICM, AUC 0.7 — Chemscore+ICM, A ————————————————————————————————————	AUC = 0.849 762	
0.0 7 0.0 0.2 0.4 False positvie	0.6 0.8 1.0 1.2 rate (1 - Specificity)		

Figure 4. Comparison of different docking software on the FIPV main protease validation dataset

The 2nd filtered compounds were characterized the interactions of protein–ligand complexes in order to identify how the compounds or ligands interact with their protein targets. The metabolic sites and protein–ligand interaction are presented in Table 1 of Appendix.

In this study as mentioned in the propose of study, the 2nd filtered compounds of the top rank were defined as the compounds in focus which were used for further tests as stated in the objective 2.

Objective 2: To evaluate the candidate compounds for their inhibitory activity against FIPV replication *in vitro* using cell-based assay.

1) FIP3CL^{pro} construction and the inhibition assay

Construction of FIP3CL^{pro} was carried out as mentioned above. The results showed that FIP3CL^{pro} has 32 KDa and its purity was more than 90% as shown in Figure 5. The enzyme concentration is 0.11 mg/ml using Bradford protein concentration assay (BioRad, USA). The protein was used in the next experiment.

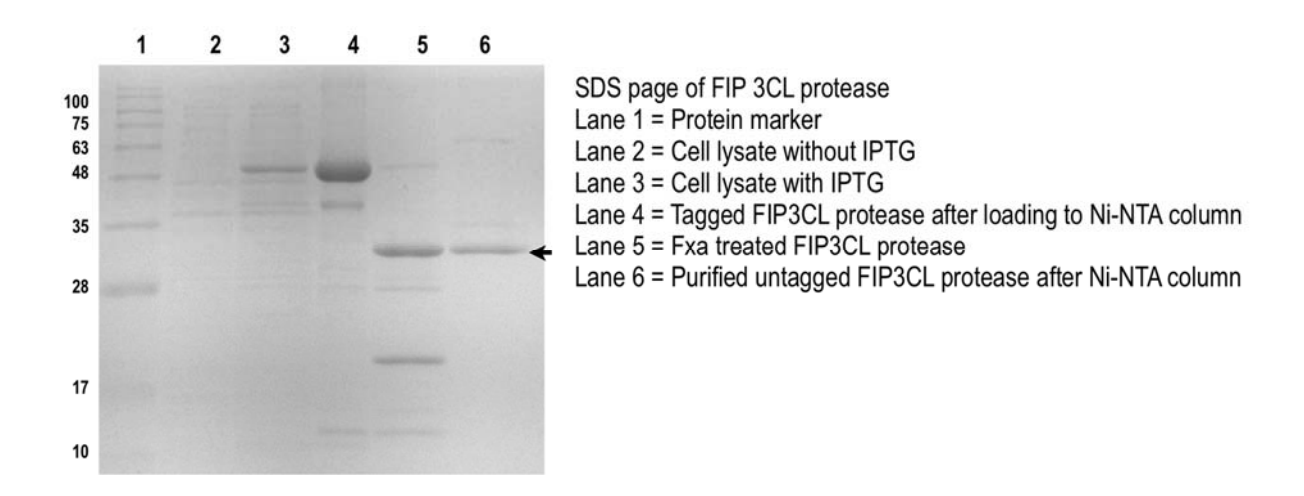


Figure 5. SDS-PAGE analysis of FIP3CL pro from the different steps of the protein purification procedure

The enzyme kinetics of FIP3CL^{pro} results showed that the purified FIP3CL^{pro} could cleave the fluorogenic peptide which as easily monitored in real time by using the fluorescence plate reader. The calculated values included; Km = $8.56\pm1.15~\mu$ M, Kcat = $0.71\pm0.04~s^{-1}$, and Vmax = $0.0247~\pm~0.00149~\mu$ M/sec, and Kcat/Km ratio = $8.29\pm0.034~M^{-1}s^{-1}$, respectively, using KaleidaGraph computer program (PA, USA). The Michaelis-Menten curve describes the relationship between the FIP3CL^{pro} enzyme (at constant concentration) and different concentrations of the fluorogenic substrate [S]. V (μ M/sec) is the initial rate of the enzyme production. The plot of the initial velocity rate of FIP3CL protease is shown in Figure 6.

Inhibitory activities of the candidate compounds for FIP3CL^{pro} were tested. The results of protease inhibition assay showed that concentrations of compound 1 and 2, which caused 50% protease inhibition (50% inhibitory concentration; IC₅₀) were less than 10 μ M. The IC₅₀ of compound 6 has around 10 μ M (Table 4).

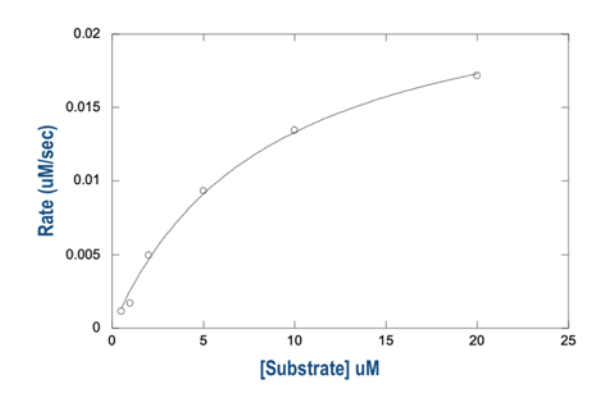


Figure 6. The enzyme kinetics of FIP3CL protease. The initial rates of the protease reaction under the different concentrations of the fluorogenic substrate were plotted against the substrate concentrations to obtain the Vmax and Km values of the enzyme.

2) Cell-based assay

2.1) Cytotoxicity assay using MTS

For cell cytotoxicity assay, the results revealed that concentrations of eight of twenty compounds that caused 50% cytotoxicity (cytotoxic concentration; CC50) were higher than 500 μ M. The concentrations were also higher than those IC₅₀ values obtained from the protease inhibitory assay, with the exception of compounds 4 and 5. Therefore, if the IC₅₀ is less than CC₅₀, the compounds could inhibit the virus while less cell toxicity. The IC₅₀ and CC₅₀ of these compounds are shown in Table 4.

2.2) Viral propagation and titration

FIPV strain 79-1146 was propagated onto CRFK cells. FIPV specific CPE included syncytial and giant cell formation followed by rapid rounding and detachment of the infected cells. The calculated viral titer was around 107.25 TCID50/ml; therefore, the virus stock was produced by further propagation in CRFK cells. Viral antigen was detected by IPMA.

The results shown that antigen-antibody reaction was literally detected from the fifth passage of FIPV strain 79-1146 infected CRFK cells. At the virus dilution of 10-1 to 10-2, most of the infected CRFK cells died, while dilutions of 10-3 to 10-6, the infected CRFK cells were still alive and presented the FIPV antigens within their cytoplasm. The presenting FIPV antigens were faint or negative at the viral dilution of 10-6 and 10-7 (Figure 7).

To determine, the optimal concentration of FIPV for cell-based antiviral assay, the experiments were performed on CRFK cells (1x105 cells/ml and 5x105 cells/ml) and two viral concentrations (100 TCID50 and 1000 TCID50). The results showed that, at 24 hpi, numbers of living CRFK cells in the mock- and FIPV-infected wells were not different

(Table 5). At 48 hpi, the numbers living cells in the infected wells were decreased with the range of 68.6–75.1% as shown in Table 5 and Figure 8 and 9. Therefore, the optimal concentration for the cell-based assay was seeding CRFK cells at 1x105 cells/ml (100 μ l/well), inoculating with FIPV at 1000 TCID50/well and evaluating the results at 24 and 48 hpi.

Table 4. FIP3CL protease inhibitory activity (IC_{50}) and cytotoxicity (CC_{50}) of the candidate compounds

Compound	Code number	IC ₅₀ (μM) ^a	CC ₅₀ (μM) ^b
1	NSC345647	6.36 ± 2.15	10.53 ± 0.13
2	NSC282187	3.57 ± 0.36	510.7 ± 0.13
3	NSC87511	29.42 ± 4.66	371.9 ± 0.26
4	NSC629301	16.14 ± 2.76	13.25 ± 0.03
5	NSC343256	24.59 ± 8.97	11.07 ± 0.08
6	CID3821945	10.32 ± 2.57	306.80 ± 0.18
7	CID452967	>500	449.80 ± 0.07
8	CID 5748601	77.20 ± 13.80	425.30 ± 0.13
9	ZINC12766300	>500	170.20 ± 0.09
10	CID5318214	28.50 ± 4.20	339.30 ± 0.03
11	CID5372747	78.40 ± 2.60	336.20 ± 0.13
12	NSC201631	97.45 ± 1.40	>500
13	NSC71097	25.90 ± 14.80	29.84 ± 0.50
14	NSC634396	>500	>500
15	NSC38273	>500	>500
16	NSC401077	>500	>500
17	NSC135168	172.40 ± 22.70	>500
18	NSC37838	>500	>500
19	CID37542 (Ribavirin)	NA°	>500
20	CID92727 (Lopinavir)	224.81 ± 43.90	>500

Note: athe concentration of the compounds that inhibited 50 percent of FIP3CL protease activity.

^bthe concentration of the compounds that have the cytotoxic effect to 50 percent of the CRFK cells.

^cnot applicable.

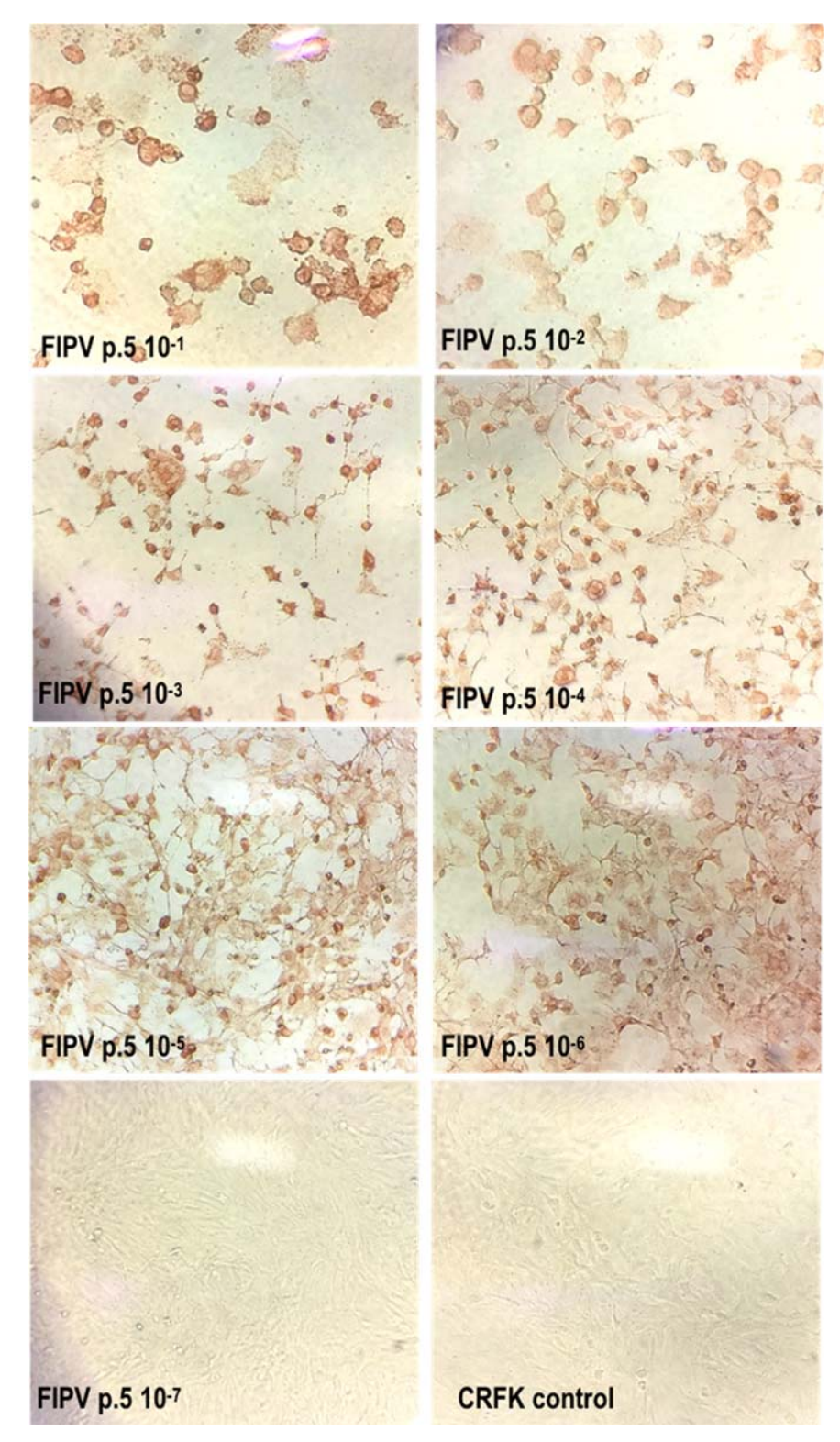


Figure 7. The IPMA results from the fifth passage of FIPV. The brown, fine intracytoplasmic granule appearance is FIPV antigens in the infected CRFK cells. The CPE appeared as multinucleated and giant cells, which was rounded-up after 48 hpi (X20 magnification).



Figure 8. CRFK cells infected with FIPV at 100 $TCID_{50}$ and 1000 $TCID_{50}$ for 24 hours

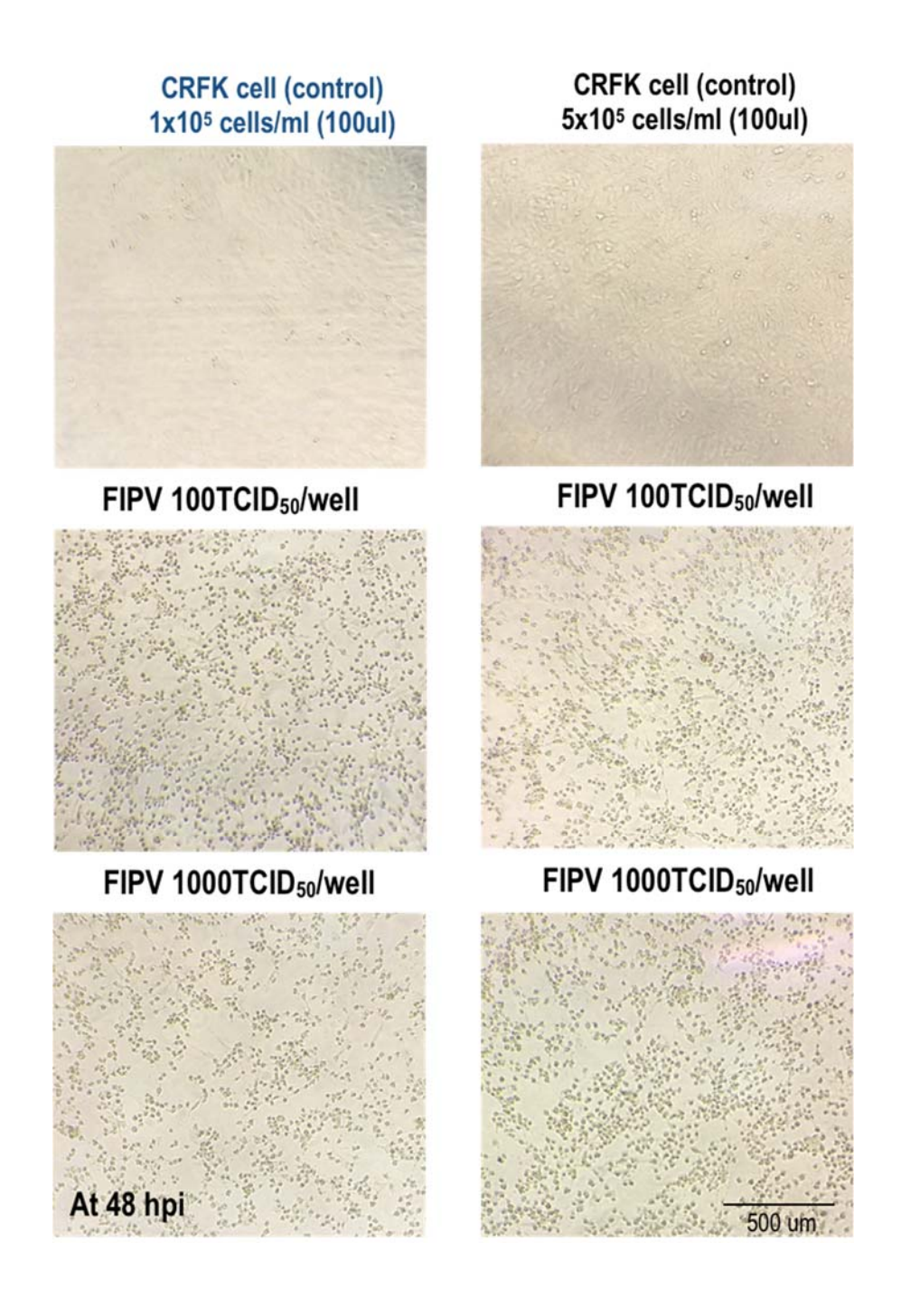


Figure 9. CRFK cells infected with FIPV at 100 $TCID_{50}$ and 1000 $TCID_{50}$ for 48 hour

Table 5. The percent of viable cells after inoculation with FIPV at 100 $TCID_{50}$ and 1000 $TCID_{50}$ for 24 – 48 hours

		2	4h			48h					
CRFK	Mean	%									
1x10 ⁵ cells/m	(490nm	Viable	5x10 ⁵ cells/m	(490nm	Viable	1x10 ⁵ cells/m	(490nm	Viable	5x10 ⁵ cells/m	(490nm	Viable
Ι (100 μ Ι))	cells	Ι (100 μ Ι))	cells	Ι (100 μ Ι))	cells	Ι (100 μ Ι))	cells
Control	1.524	100	Control	1.638	100	Control	1.306	100	Control	1.518	100
100TCID ₅₀	1.535	100.7	100TCID ₅₀	1.834	112.0	100TCID ₅₀	1.350	103.3	100TCID ₅₀	1.140	75.1
1000TCID ₅₀	1.364	90.2	1000TCID ₅₀	1.711	104.5	1000TCID ₅₀	0.896	68.6	1000TCID ₅₀	1.095	72.1

2.3) Antiviral activity assay

In order to determine the inhibition activity of the compounds to FIPV infection on CRFK cells, the studies ere into three conditions of the viral infection. At experiments least 3 were performed with two biological replications for each concentration of the compound. We evaluated the viral infection based on the differential expression of FIPV antigens within cytoplasm of mock- and virus-infected CRFK cells.

Antiviral activity during the pre-viral entry step was determined whether or not the compounds could inhibit the virus before it entered into the host cell. Compounds 1, 3, 4, 5 and 13 demonstrated the good inhibitory activity when compared to ribavirin, board spectrum antiviral drug. In addition, the compounds 1, 4, 5 and 13 had better EC_{50} values than the referent protease inhibitor (lopinavir). However, the compounds 2 and 6 could not inhibit FIPV entry, even if they had good IC_{50} values. The selective index (SI) of compounds 1, 3, 13, and 18 were higher than 4.00.

The study on antiviral activity during post-viral entry step of FIPV infection revealed that same compounds could inhibit FIPV replication after viral entry and FIP3CL protease was expressed. The results showed that compounds 1, 3, 4, 5, 13 and 18 had good EC_{50} values; in particular, compounds 5, 13 and 18 had better EC_{50} values than when tested under the pre-viral entry study. The compound 3 had only good SI value as shown in Table 6.

The prophylactic antiviral activity for FIPV infection was determined whether or not the small molecular compounds could penetrate into the host cells and also still had inhibitory activity to prevent FIPV infection. The results revealed that the compounds 1, 4, 5 and 13 still had good protection. However, their SI values were quite lower. Surprisingly, compound 18 had better prophylaxis than other activities. However, it possessed very high IC $_{50}$ values (> 500 μ M) in the protease inhibitory assay. The EC $_{50}$ values and the morphology and antigen presentation of FIPV infected cells when examined under three conditions were shown in Table 6 and Figures 10 - 12. In conclusion, the compound 1 possessed the best inhibitory activity for FIPV infection in all three conditions. The compounds 1, 3, 4, 5 and 13 were selected for further experiments to evaluate the viral quantities.

3) Examination of FIPV inhibition activity of compounds by RT-realtime qPCR

RT-realtime qPCR was used to determine viral quantity in each experiment. The results of qPCR efficacy for each condition, the standard curve of using copy numbers of plasmid containing FIP-3'UTR sequence and the melting curve analysis were shown in Figures 1 – 4 in the Appendix. The viral quantity was determined by absolute quantification based on the standard curve of the viral copy numbers. The RT-qPCR results were corresponded to the intensity of the viral antigens as detected by IPMA (Figures 13 –15).

4) Molecular dynamic simulation of the best compounds

According to our results, the compound 1 displayed a good inhibitiory effect on the protease activity of FIP3CL ^{pro} (IC₅₀ = 6.36 \pm 2.15 μ M), a promising antiviral activity as well (EC₅₀ =1.186 to 4.867 μ M), and a low CC₅₀ value (CC₅₀ = 10.53 \pm 0.13 μ M). Therefore, the complex of FIP3CL^{pro}–compound 1 was selected for molecular dynamic simulation to observe the dynamic interaction between the molecules ant the FIP3CL^{pro} protein.

Molecular dynamic simulation experiment was generated in 2 ns MD trajectories for initial configuration. The Root mean square displacement (RMSD) of the complex structure of system was performed to reach equilibrium after final 6 ns. The overall RMSDs were analyzed and plotted. The RMSD values of compound 1 were the minimum at 1.9048 Å to the maximum at 3.4476 Å. For FIP3CL protease, the RMSDs of all atoms was the minimum at 1.2366 Å to the maximum at 2.0395 Å, and the backbone of FIP3CL protease was the minimum at 1.1154 Å to the maximum at 2.5211 Å, respectively. The

compound 1 in the FIP3CL^{pro}–cpd 1 complex was slightly different from at equilibration (Figure 16).

The FIP3CL^{pro}–cpd1 complex interaction was analyzed using the bond to bond interaction of hydrogen bond and the others such as, electrostatic and van der Waals interaction between protein–ligand in the binding pocket. The residues were carried out based on the following criteria: 1) proton donor–acceptor distance 2) donor–H acceptor bond angle and their interactions as shown in the Tables 6 -7 and Figure 17. The HIS41 and CYS144 residues of 3CL protease, which is the common active sites of CoV, were found to interact with the compound 1 by alkyl bond and hydrogen bonds.

In conclusion from our results, it could be suggested that the compound 1 is the promising protease inhibitor that could prevent the FIPV infection probably targeting the $FIP3CL^{pro}$. However, the other compounds with high EC_{50} values and good SI values could be good candidate compounds as well.

Table 6. The EC_{50} and the SI values of the pre-viral-, the post-viral entry, and the prophylactic activities for FIPV infection of lead compounds

O 4		Previral	entry	Postvira	l entry	Prophylaxis		
Cpd	Code number	IPMA	Selective	IPMA	Selective	IPMA	Selective	
number		EC ₅₀ (μM)	Index (SI)	EC ₅₀ (μM)	Index (SI)	EC ₅₀ (μΜ)	Index (SI)	
1	NSC345647	1.186 ± 0.954	8.880	4.867 ± 0.115	2.208	2.851 ± 0.520	2.693	
2	NSC282187	>100	N/A	>100	N/A	>200	N/A	
3	NSC87511	16.24 ± 1.334	22.901	21.829 ± 1.635	17.037	>200	N/A	
4	NSC629301	7.753 ± 0.447	1.709	6.203 ± 0.876	2.136	6.11 ± 1.899	2.169	
5	NSC343256	3.834 ± 0.438	3.887	4.002 ± 0.370	2.766	16.222 ± 1.226	0.682	
6	CID3821945	>100	N/A	>100	N/A	>100	N/A	
7	CID452967	>200	N/A	>100	N/A	>200	N/A	
8	CID 5748601	>100	N/A	>100	N/A	>200	N/A	
9	ZINC12766300	>200	N/A	>100	N/A	>200	N/A	
10	CID5318214	>100	N/A	>100	N/A	>200	N/A	
11	CID5372747	>100	N/A	>100	N/A	>200	N/A	
12	NSC201631	>100	N/A	>100	N/A	>100	N/A	
13	NSC71097	4.030 ± 0.595	7.40	2.34 ± 0.96	2.208	1.998 ± 0.301	3.693	
14	NSC634396	>100	N/A	>100	N/A	>100	N/A	
15	NSC38273	>100	N/A	>100	N/A	>100	N/A	
16	NSC401077	>100	N/A	>100	N/A	>100	N/A	
17	NSC135168	>100	N/A	>100	N/A	>100	N/A	
18	NSC37838	78.52 ± 1.178	>100	31.951 ± 1.372	>100	76.011 ± 4.76	>100	

19	CID37542 (Ribavirin)	48.867 ± 1.774	25.682	73.984 ± 0.183	16.963	>200	N/A
20	CID92727 (Lopinavir)	8.560 ± 0.474	61.519	5.383 ± 2.318	97.832	31.70 ± 1.366	16.612

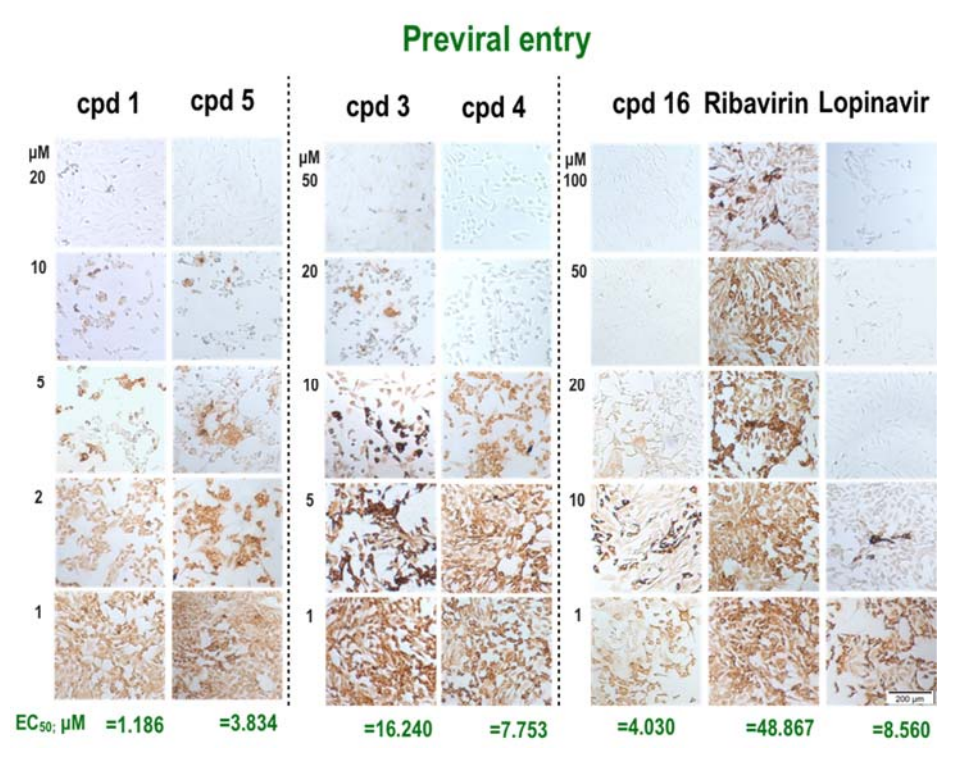


Figure 10. IPMA demonstrating the presence of viral antigens in the FIPV-infected CRFK cells treated with tested compounds and drug control under pre-viral entry condition

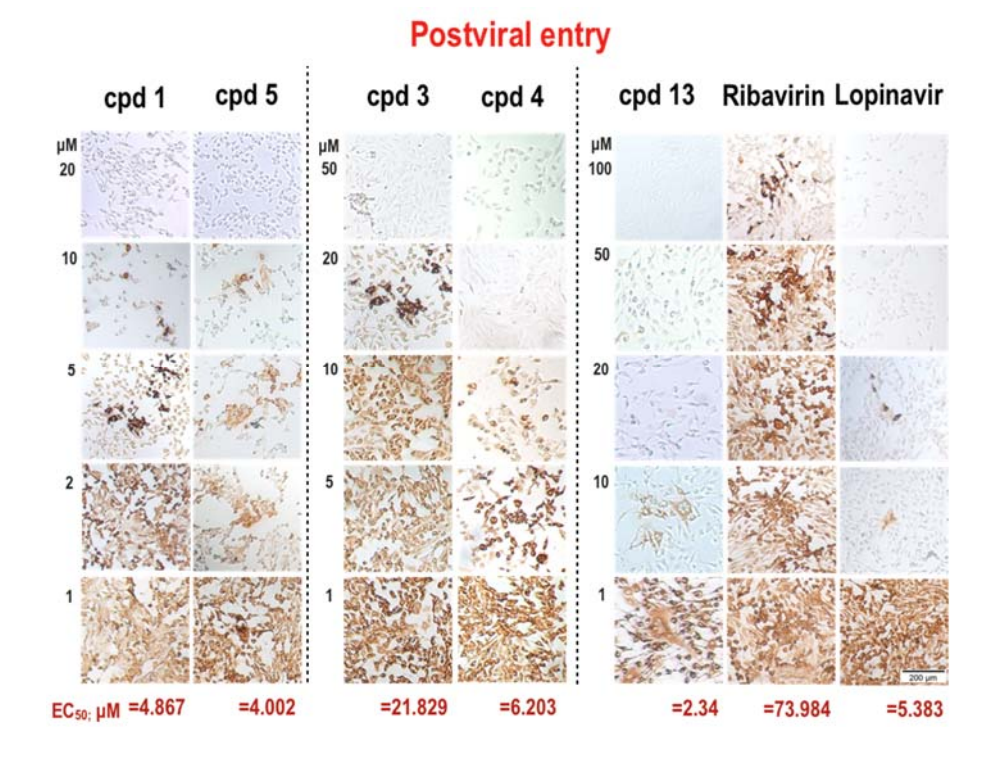


Figure 11. IPMA demonstrating the presence of viral antigens in the FIPV-infected CRFK cells treated with tested compounds and drug control under post-viral entry condition

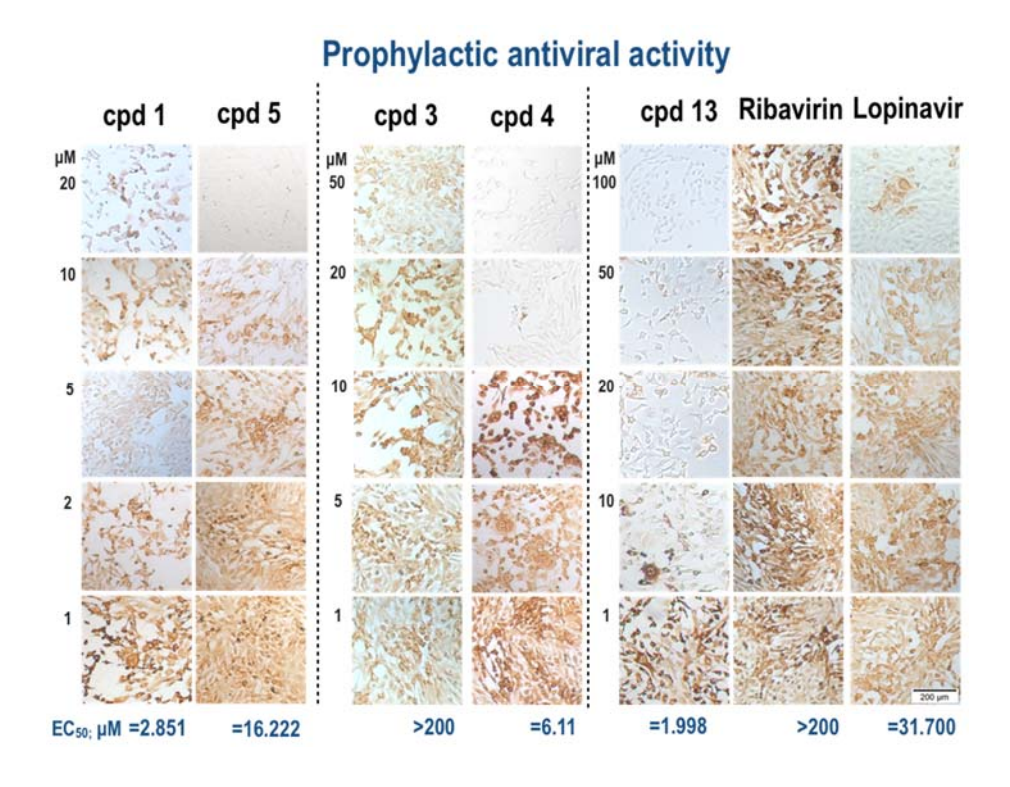


Figure 12. IPMA demonstrating the presence of viral antigens in the FIPV-infected CRFK cells treated with tested compounds and drug control under prophylactic antiviral condition

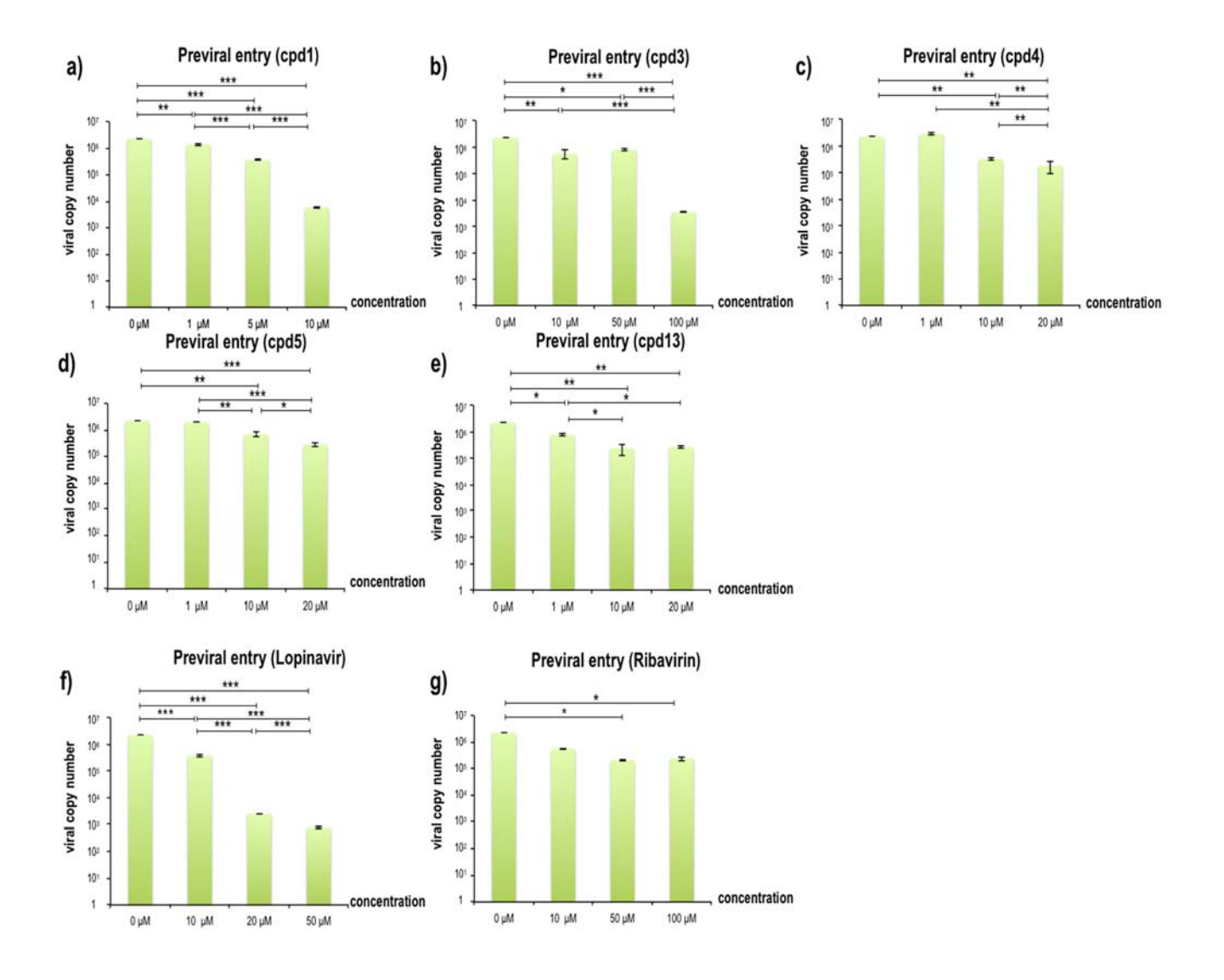


Figure 13. Realtime qPCR for determination of FIPV quantity after compound treatment under the pre-viral entry condition (a-g). Various concentrations of the compounds 1 (a), 3 (b), 4 (c), 5 (d), 13 (e), lopinavir (f) and ribavirin (g) are examined to demonstrate their dose-response effects.

The asterisks are *=p < 0.05, **=p < 0.01, ***=p < 0.001, respectively.

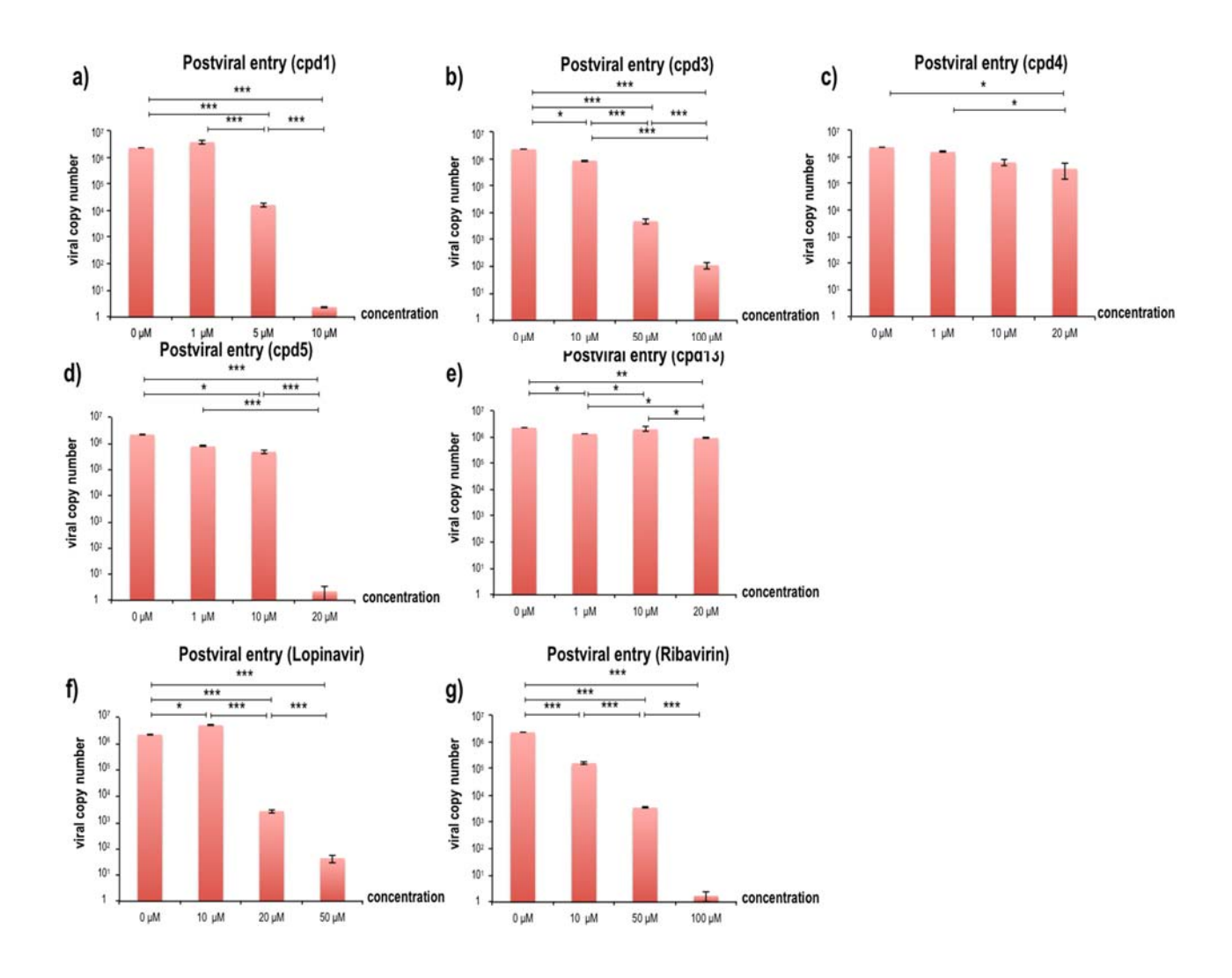


Figure 14. Realtime qPCR for determination of FIPV quantity after compound treatment under the post-viral entry condition (a-g). Various concentrations of the compounds 1 (a), 3 (b), 4 (c), 5 (d), 13 (e), lopinavir (f) and ribavirin (g) are examined to demonstrate their dose-response effects.

The asterisks are *=p < 0.05, **=p < 0.01, ***=p < 0.001, respectively.

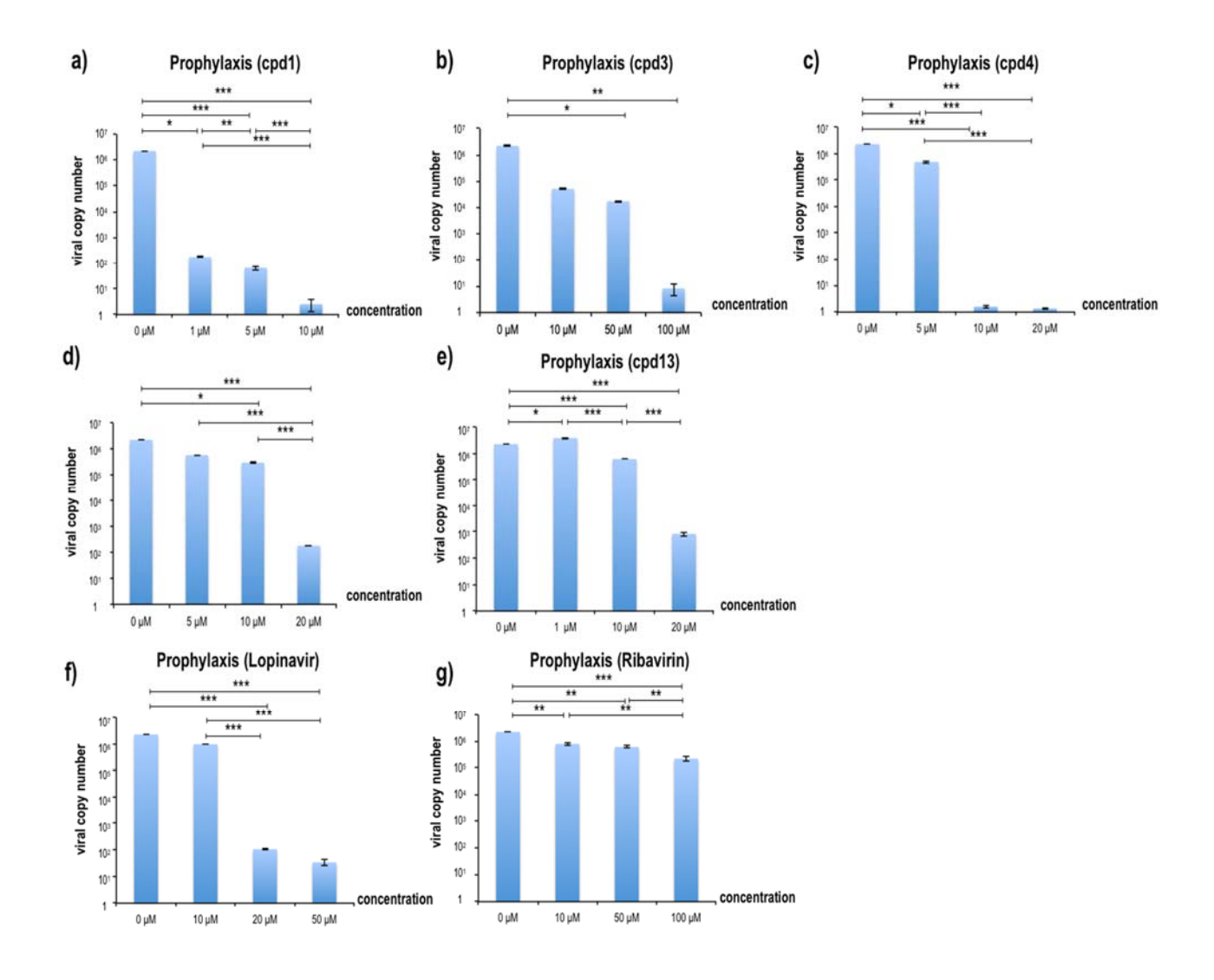


Figure 15. Realtime qPCR for determination of FIPV quantity after compound treatment under the prophylactic anitiviral condition (a-g). Various concentrations of the compounds 1 (a), 3 (b), 4 (c), 5 (d), 13 (e), lopinavir (f) and ribavirin (g) are examined to demonstrate their dose-response effects. The asterisks are * = p < 0.05, ** = p < 0.01, *** = p < 0.001, respectively.

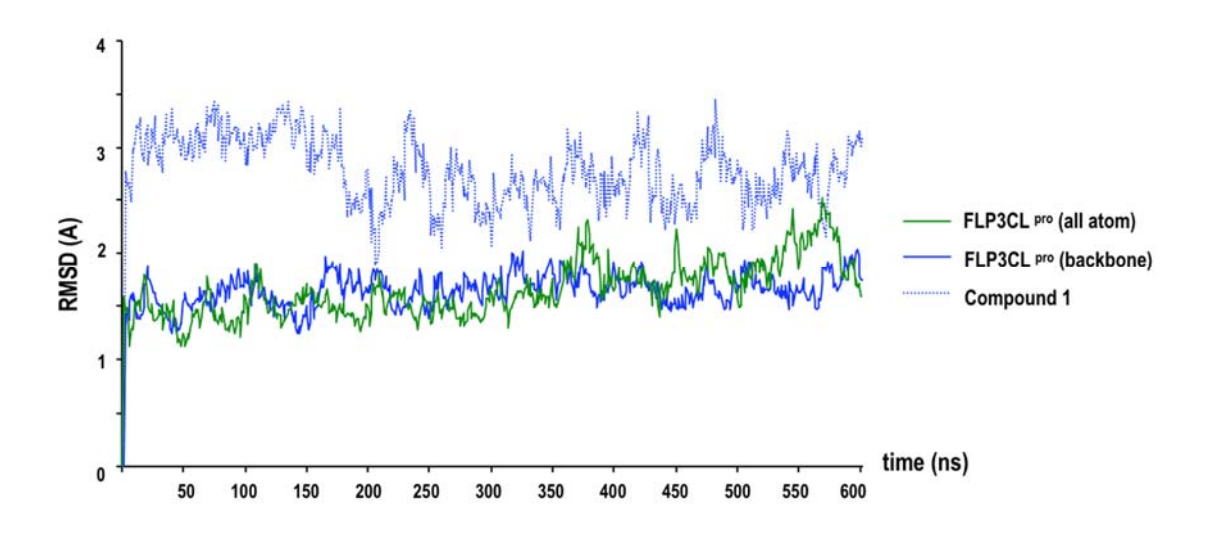


Figure 16. RMSD curves of the overall atoms (green), the backbone (blue), and compound 1 (blue dash) of FIP3CL pro-compound 1 complex

Table 6. Hydrophobic interaction of FIP3CL-cpd1 complex

Residu	ıe	Distance	Ligand atom	Protein atom	Ligand coordination	Protein coordination
ALA	141	3.99	10	1387	-44.426, -14.831, -4.480	-44.615, -15.024, -0.500
GLU	165	3.86	22	1607	-48.442, -17.118, -8.406	-46.590, -20.492, -8.145
PRO	188	3.67	32	1811	-47.834, -12.808, -12.074	-51.300, -12.311, -13.176

Table 7. Hydrogen bonds as well as donor and acceptor atoms of FIP3CL-cpd1 complex

Residu	ue	Distance between Hydrogen atom to acceptor atom	Distance between donor to acceptor atom	Donor Angle	Protein donor	Side chain	Donor atom	Acceptor	Ligand coordination	Protein coordination
ILE	140	2.1	3.02	161.02	Х	Х	45[O3]	1377[O2]	-42.145, -15.555, -3.812	-41.227, -17.371, -1.582
GLY	142	1.91	2.8	144.2	1	Х	1388[Nam]	43[O3]	-43.254, -13.149, -3.230	-41.442, -14.186, -1.366
THR	143	2.39	3.25	140.31	1	Х	1393[Nam]	45[O3]	-42.145, -15.555, -3.812	-39.185, -15.184, -2.532
CYS	144	3.22	3.71	111.12	1	Х	1402[Nam]	45[O3]	-42.145, -15.555, -3.812	-38.817, -14.676, -5.192
HIS	162	2.97	3.97	168.2	1	1	1578{Npl]	41[O3]	-44.738, -18.644, -6.204	-41.146, -19.101, -7.843
GLU	165	2.59	3.11	114	x	1	35[O3]	1610[O2]	-47.508, -18.367, -4.521	-47.606, -21.409, -5.158
GLU	165	3.18	3.7	115.89	x	1	41[O3]	1611[O2]	-44.738, -18.644, -6.204	-45.539, -22.159, -5.351

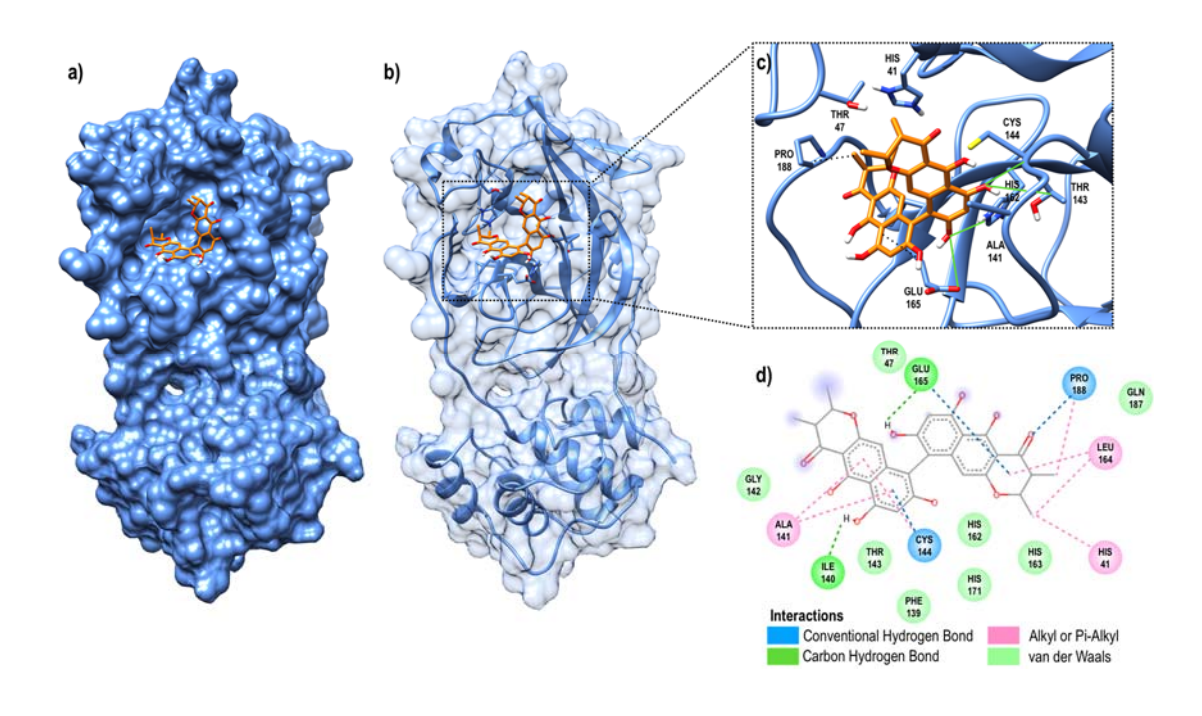


Figure 17. The FIP3CIL ^{pro}—compound 1 complex a-b) compound 1 in the binding pocket of FIP3CL ^{pro} (blue surface and blue ribbon), 3D- (c) and 2D- (d) structure of the complex interactions

Discussion

In this study, we used the structure-based virtual screening as a powerful tool for screening potential lead compounds. In this approach, the docking programs, such as Autodock, Autodock Vina, GOLD, and ICM programs are used widely. These programs are based on the different force field calculations and algorithms [Zhang et al, 2017; Wang and Wang 2002]. Therefore, consensus scoring was used in order to significantly reduce false positive of single scoring procedure from virtual library screening and improve the hit-rate of the candidates for bioassay. We validated the accuracy of these procedures by retrieving the top-ranked compounds predicted by each programs, and then we re-evaluated by re-scoring function to calculate binding affinity of a ligand. Performances of the docking software were compared using their score distribution and the receiver operating characteristic (ROC) curves plus areas under the ROC curve (AUCs). These approaches determined performance of the candidate active molecules while discard inactive molecules [Zhang et al, 2017; Zhao, et al, 2009; Triballeau et al, 2005]. These results obtained from the ROC analysis of all three programs were consistent when compared with the single scoring for further bioassays.

Compound 1 is a fungal metabolite, called Chaetochromins, isolated from *Furasium* (Ascomycotina, Hypocreales), *Penicillium, Chaetomium*, etc. Chaetochromin A is a symmetrical dimer having two trans-2, 3-dimethyl groups on the 5, 6, 8-trihydroxy-naphtho- γ -pyrone ring [Ugaki et al, 2012; Koyoma et al, 1987]. Chaetochromins and their derivatives have been reported as HIV integrase inhibitor by using strand transfer assay of recombinant integrase with IC₅₀ = 1–12 μ M [Singh et al, 2003]. *In silico* analysis, the complex of chaetochromin and HRAS protein in the AIDS-associate cancers was simulated; the result showed that chaetochromin B was stable in the binding pocket. It can be a promising antiviral drug [Omer and Singh, 2016]. In our study, the three viral entry assays showed that chaetochromin could inhibit the FIPV infection with the good IC₅₀ and EC₅₀; however, it might have a cytotoxic effect on the host cells.

Stictic acid (compound 3) is extracted from the lichen spp (Usnea articulate, Lobaria pulmonaria, Xanthoparmelia conspersa, Xanthoparmelia camtschadalis and Ypotrachyna revolu) [White 2014; De pas etal, 2010]. Stictic acid is a β -orcinol depsidone, produced by the lichens. The characteristic and unique secondary metabolites of polyketides are commonly found in stictic acid, and contained aromatic rings. The stictic acid derivatives have been reported that it could

reduce ROS production in the cells via anti-oxidative activity [Lohèzic-Le Dèvèhat, 2007; Papadopoulou et al, 2007]. Moreover, the stictic acid could react to the Cys 141 with the cysteine triad for reducing p53 reactivation in human cancers [Wassman et al, 2013]. It should be noted that 3CL protease of the CoV contains Cys as the nucleophile active site in the catalytic triad (Cys144, and His41) as well [Kim et al, 2012; Kuo et al, 2004]. In our docking result, the compound showed the interaction to the His 41 (alkyl bond) and Cys144 (donor hydrogen bond), and we also found a good inhibition of compound 3 by the FIP3CL protease inhibition assay. The derived-stictic acid compounds and the atranorin from the lichens using acetone extraction could inhibit hepatitis C replication [Vu et al, 2015]. In addition, the stictic acid had anti-HIV-1 integrase activities with IC_{50} less than 50 μ M [Neamati et al, 1997].

Hitachimycin (compound 5), a natural compound, was firstly isolated from *Streptomyces scabriporus* [Umezawa et al, 1981]. It was also known as stubomycin, which is one of β -amino acid-containing macrolactam polyketides with β -phenylalanine at the starter units [Miyanaga et al, 2016; Kudo et al, 2015]. The hitachimycin and related compounds contained aromatic ring of β -amino acid as its polyketide skeleton, such as vicenistatin, fluvirucin A1, fluvirucin B2, cremimycin and incednine. Hitachimycin has been reported as antiprotozoal and antitumor antibiotics, but there is less report on antiviral effect [Komiyama et al, 1983]. Fluvirucins, which has a core of macrolytic similar to hitachimycin, has antiviral effect against influenza virus type A (Vitoria strain) in MDCK cell culture with IC $_{50}$ = 2 ~ 10 μ g/ml. It also had lower CC $_{50}$ values similar to our study [Naruse et la, 1991a; Naruse et la, 1991b]. From these antimicrobial evidences, polyketide synthase could synthesize each metabolite of hitachimycin and fluvirucins. Gene analysis and cluster study have been evaluated biosynthetic genes of enzymes, which contribute to biosynthetic machinery in order to develop further new compounds [Kudo et al, 2015; Lin et al, 2013].

Compound 13 (NSC71097) from National Cancer Institute (NCI) depository is a non-natural compound. The chemical structure of the compound is 1-(5-chloro-2-hydroxyphenyl)-3-(2-quinolinyl)-2-propen-1-one. It has a little information. Thus far, there is no report on the anti-HIV screening or antitumor activity. We found 3 compounds with drug likeness property had structure similar to NSC71079 in the Pubchem. These compounds were active in bioactivity assays such as binding affinity to calf thymus DNA and inhibition of human U937 cell culture with active effect of 19.3–22.5 μ M (BioAssay AID: 1259799 and 1259800). Antiprotozoal effect was reported as potency of bioactivity value of 2.3323 (Bioassay AID: 504832 and 485364). However, the details form these assays and their antiviral activities were not published yet.

Two control inhibitors in this study, Ribavirin and Lopinavir, were included in our experiments. Ribavirin is a synthetic nucleoside, a ribosyl purine analog, with antiviral activity. It could interfere with the viral entry and replication. This activity is enhanced by using combination with interferons or other antiviral drugs that synergistically inhibited the viruses rather than treated with the ribavirin alone as reports in the MERS-CoV and SARS-CoV regimens [Falzarano et al 2013; Omrani et al, 2014]. Ribavirin combination with lopinavir/ritonavir and steroids showed slight reduction of mortality rate in SARS-CoV infection [Chan et al, 2013]. Therefore, it was used as a reference compound antiviral activity of the candidate compounds as a reference compound in many viral researches. However, the mechanism of ribavirin action is still unclear and highly variable in many patients [Cameron and Castro 2001; Zulma et al, 2016]. In our study, the previral- and post-viral entry experiments showed less antiviral effect to FIPV infection (EC $_{50}$ = 48–78 μ M). Furthermore, no antiviral effect was found in the prophylaxis study.

Lopinarvir, an HIV protease inhibitor, was commonly combined with ritonavir for the treatment of HIV disease. Lopinavir and with ritonavir-booted form have antiviral activities in some clinical cases of MERS-CoV and SARS-CoV [Chan et al, 2015; Chu et al, 2004]. It was expected that lopinavir possibly contribute to the 3CL protease inhibition. However, lopinavir and derivatives partially inhibited the 3CL protease of SARS-CoV with IC $_{50}$ = 50 μ M and ~ 25 μ M, respectively [Wu et al, 2004]. This result corresponded to our protease inhibitory assay with high IC $_{50}$ values (IC $_{50}$ = 224.81 ± 43.9 μ M). Despite of having low IC $_{50}$ value, we found that lopinavir was a good inhibitor for viral entry step (EC $_{50}$ = 5–8 μ M). It is possible that lopinavir may have additional inhibitory activity to other proteases when examined by cell-based experiments. The papain-like protease 1 (PL1 pro), a common protease in CoV, has a fingers subdomain and a catalytic triad, Cys32-His183-Asp196, which these residues and PL1 pro domainwere found only in the alpha-CoV (TGEV), but absent in beta-coronavirus (Lei et al, 2018). For other host protease, such as Furin protease, Lopinavir might be involved via blocking furin-mediated cleavage during viral entry. Thus, the mechanism of lopinavir action on FIPV infection is still further investigated.

The selectivity index (SI), defined as the ratio of the CC_{50} to the EC_{50} was used to determine drug selectivity. We use an SI value ≥ 4 as the definition of "hits" compounds according to Severson et al (2007). Our study showed that SI value of compound 1 was 8.880 for the previral entry assay. However, for the post-viral entry and prophylactic antiviral activity, it had showed SI = 2.208 and 3.693, respectively, with binding affinity of -12.2 kcal/mol using Autodock Vina. In addition, the compound 3 had SI values higher than 4 for both of the previral- (SI = 22.901) and postviral entry (SI = 17.037) assays; however, for the prophylaxis assay, it did not show any

inhibition. Therefore, compounds 1 and 3 could be promising candidate of natural compounds for drug development. NSC71097 is also a good candidate to further develop drug prototype or the modified form.

Regarding inactive compounds, compounds 2 and 6 showed a good protease inhibition, but they could not inhibit FIPV infection in the cell-based assay. Compound 2 (NSC282187) is carbamic acid, (4-fluorophenyl)-, 1,2-dihydro-2-oxo-3-pyridinyl ester. Up to date, there is no report of antimicrobials and anticancer activities of this compound. We found that the binding affinity between compound 2 and FIP3CL^{pro} was -7.2 kcal/mol with IC₅₀ = 3.569 \pm 0.3634 μ M, and CC₅₀ > 500 μ M. Compound 6 is an isatin derivative [Chen et al., 2005]. Isatin derivatives have been reported as a 3CL^{pro} inhibitor for SARS-CoV [Chen et al., 2005; Zhou et al., 2006, Kuo and Liang, 2015]. It was a potent inhibitor against the rhinovirus 3C^{pro} [Webber et a, 1996]. In our molecular docking analysis, we found that this compound could be in the binding pocket of FIP3CL^{pro} with very good binding affinity (-13.5 kcal/mol). The binding involves hydrophobic interaction through Leu27, His41, Thr47, Leu164 and Pro188, hydrogen bond of Val26 and Pi-stacking at His41, respectively. We also found a good FIP3CL inhibition of compound 6 by using protease inhibitory assay. However, both compounds did not show any antiviral activity in all three conditions of cell-based assay. It is possible that their anti-protease activities might be affected by unknown factors within the cell-culture circumstance.

Coronaviruses is infect and cause diseases in animals and human. Viruses such as porcine transmissible gastroenteritis virus (TGEV), avian infectious bronchitis virus (IBV), bovine coronavirus (BCoV) and feline infectious peritonitis (FIPV) cause severe diseases in animals. Severe acute respiratory syndrome (SARs) causes by a coronavirus namely SARs-CoV. After the first outbreak, it spread rapidly in Asia [Chow et al, 2003]. All members in CoV possess 3C-like protease, with a common 3D structure that is mostly resemble to 3C protease of piconaviruses and noroviruses [Kuo et al, 2009].

Therefore, 3CL^{pro} is the one of specific target of the inhibitors. In case of FIPV, the 3CL^{pro} contains a Cys residue as the nucleophilic active site in the catalytic dyad (His41 and Cys144 residues) [Wang et al, 2016: St.John et al, 2015]. The drug design of 3CL^{pro} inhibitors is to incorporate an electrophilic moiety that contributes to covalent bond between the catalytic cysteine residue and the inhibitor. Therefore, the most structures of the inhibitors usually contain the nucleophilic moiety for sharing the electrons to the carbonyl residue for covalent bond formation between inhibitor and enzyme. The functional groups are commonly termed 'warhead', which is based on a carbonyl group (Tiew et al, 2011). The researcher on FIP3CL^{pro} has developed inhibitors containing dipeptidyl residue with different warheads (Kim et al, 2012, Kim

et al, 2013). The dipeptidyl aldehyde has one of carbonyl group with nucleophile that can donate a pair of electrons. As a consequence by the nucleophilic attack, hydrolysis of the key catalytic group occurs in the active site of 3CL^{pro}. In our study, we found that most candidate compounds contained a carbonyl group, which has a predilection for the active site of FIP3CL^{pro}. According to molecular docking analysis, all compounds except compounds 12, 17 and 18 have interactions with His41 or Cys144 in the binding pocket. Compounds 1-6 and 13 are good for direct inhibition to FIP3CL protease. However, the functional groups of some compounds might show an inactive or less function in the environment of cell-culture.

Conclusion

This study demonstrated the application of computer-based assay on virtual screening in order to find a good antiviral candidate for FIPV treatment. We have targeted the FIP3CL ^{pro}, which responsible for CoV poly-protein processing during viral replication. The available drug libraries from NCI, Pubchem and Zinc databases were retrieved for virtual screening by homology modeling and molecular docking. The selected small molecules were tested for protease inhibition and cell-based assay. We could find at least 3-4 compounds, which are very good antiviral candidates and could be precursor molecules for further drug development.

Acknowledgements

This research was supported by Thailand Research Fund (TRF) [grant number MRG6080067]. I thank my colleagues from Faculty of Veterinary Medicine, Kasetsart University who provided insight ful information that greatly assisted the research. I appreciated my mentor, Prof. Dr. Porntippa Lekcharoensuk for her guidance, critical comments and support throughout the study and Asst. Prof. Dr. Chih-Jung from National Chung Hsing University, Taiwan for protease inhibitory assay that increases quality of this research. I would also like to show my gratitude to Assoc Prof Dr Kiattawee Choowongkomon, Faculty of Science, Kasetsart University and Dr. Sissades Tongsima, Head of Biostatistics and Informatics Laboratory, Genome Institute, BIOTEC, Thailand for sharing their computer softwares during this research. Finally, I thank the members of PL lab, especially a Ph.D student, Mr. Nattarat Thangthamniyom and a research assistant, Miss Nantawan Petcharat for their advises and collaboration.

References

- Abagyan et al, 1994. ICM a new method for protein modeling and design. Applications to docking and structure prediction from the distorted native conformation. J. Comp. Chem. 15: 488-506.
- 2. Bálint et al, 2014. Recombinant feline coronaviruses as vaccine candidates confer protection in SPF but not in conventional cats. Veterinary Microbiology. 169:154–162.
- 3. Berry et al, 2015. Potential broad spectrum inhibitors of the coronavirus 3CL^{pro}: a virtual screening and structure-based drug design study. Viruses. 7: 6642–6660.
- Cameron and Castro, 2001. The mechanism of action of ribavirin: lethal mutagenesis of RNA virus genomes mediated by the viral RNA-dependent RNA polymerase. Curr Opin Infect Dis. 12: 261–272.
- Chan et al, 2003. Treatment of severe acute respiratory syndrome with lopinavir/ritonavir: a multicentre retrospective matched cohort study. Hong Kong Med. J. 9: 399–406.
- 6. Chen et al, 2005. Synthesis and evaluation of isatin derivatives as effective SARS coronavirus 3CLprotease inhibitors. Bioorg Med Chem Lett. 15: 3058–3062.
- 7. Chen et al, 2006. On evaluating molecular-docking methods for pose prediction and enrichment factors J Chem Inf Model. 46(1): 401-415Dedeurwaerder et al, 2013. The role of accessory proteins in the replication of feline infectious peritonitis virus peripheral blood monocytes. Veterinary Microbiology. 162:447–455.
- 8. Chow et al. 2003. Molecular advances in severe acute respiratory syndrome-associated coronavirus (SARS-CoV). Genomics Proteomics Bioinformatics. 1(4):247-62.
- 9. Chu et al, 2004. Role of lopinavir/ritonavir in the treatment of SARS: initial virological and clinical findings. Thorax. 59: 252–256.
- 10. Cinatl, J. et al. 2003. Treatment of SARS with human interferons. Lancet. 362: 293-294
- 11. Chang et al, 2010. Feline infectious peritonitis: insights into feline coronavirus pathobiogenesis and epidemiology based on genetic analysis of the viral 3c gene. Journal of General Virology. 91:415–420.
- Dallakyan and Olson, 2015. Small-molecule library screening by docking with PyRx. Methods Mol Biol. 1263: 243-250.
- De Paz et al, 2010. HPLC isolation of antioxidant constituents from Xanthoparmelia spp.
 J. Pharm. Biomed. Anal. 53: 165–171.
- 14. Desmarets et al, 2013. Establishment of feline intestinal epithelial cell culture for the propagation and study of feline enteric coronaviruses. Veterinary research. 44: 71.

- 15. Fehr et al, 1997. Placebo-controlled evaluation of a modified life virus vaccine against feline infectious peritonitis: safety and efficacy under field conditions. Vaccine. 15:1101–1109.
- 16. Falzarano et al, 2013. Treatment with interferon-a2b and ribavirin improves outcome in MERS-CoV-infected rhesus macaques. Nature Medicine. 19(10): 1313–1317.
- 17. Ferreira et al, 2014. Molecular docking and structure-based drug design strategies. Molecules. 20: 13384–13421.
- 18. Foley et al, 1997. Risk factors for feline infectious peritonitis among cats in multiple-cat environments with endemic feline enteric coronavirus. Journal of American Veterinary Medical Association. 210:1313–1318.
- 19. Gamble et al, 1997. Development of a nested PCR assay for detection of feline infectious peritonitis virus in clinical specimens. Journal of Clinical Microbiology. 35(3): 673–675.
- 20. Hartmann K, 2005. Feline infectious peritonitis. Veterinary Clinical Small Animal. 35:39–79.
- 21. Hartmann and Ritz, 2008. Treatment of cats with feline infectious peritonitis. Vet immunology and Immunopathlogy. 123: 172–175.
- 22. Hsieh et al, 2010. Synergistic antiviral effect of *Galanthus nivalis* agglutinin and nelfinavir against feline coronavirus. Anitiviral Research. 88: 25–30.
- 23. Jain and Nicholls, 2008. Recommendations for evaluation of computational methods. Journal of Computer-Aided Molecular Design. 22(3–4): 133–139.
- 24. Jones et al, 2002. Development and validation of a genetic algorithm for flexible docking. Journal of Molecular Biology. 267(3): 727–748.
- 25. Kennedy et al, 2001. Deletions in the 7a ORF of feline coronavirus associated with an epidemic of feline infectious peritonitis. Veterinary Microbiology. 81(3): 227–234.
- 26. Kim et al, 2012. Broad-Spectrum Antivirals against 3C or 3C-Like Proteases of Picornaviruses, Noroviruses, and Coronaviruses. Journal of Virology. 86(21): 11754–11762.
- 27. Kim et al, 2013. Potent inhibition of feline coronaviruses with peptidyl compounds targeting coronavirus 3C-like protease. Anitiviral Research. 97:161–168
- 28. Kirchmair et al, 2011. Development of anti-viral agents using molecular modeling and virtual screening techniques. Infectious Disorders-Drug Targets. 11:64–93.
- 29. Kipar and Meli, 2014. Feline infectious peritonitis: still an Enigma?. Veterinary Pathology. 51(2): 505–526.

- 30. Komiyama et al, 1983. Studies on the biological activity of stubomycin. The Journal of Antibiotics. 36(3): 301–311.
- Koyama et al, 2011. Absolute configurations of chaetochromin A and related bis(naphtho-.GAMMA.-pyrone) mold metabolites. Chemical & Pharmaceutical Bulletin. 35(10), 4049–4055.
- 32. Kudo et al, 2015. Genome Mining of the Hitachimycin Biosynthetic Gene Cluster: Involvement of a Phenylalanine-2,3-aminomutase in Biosynthesis. ChemBioChem, 16(6): 909–914.
- 33. Kuo et al 2004. Characterization of SARS main protease and inhibitor assay using a fluorogenic substrate. Biochemical and Biophysical Research Communications. 318: 862-867.
- 34. Kuo et al, 2009. Individual and common inhibitors of coronavirus and picornavirus main proteases. FEBS Letters. 583(3): 549–555.
- 35. Kuo and Liang, 2015. Characterization and Inhibition of the Main Protease of Severe Acute Respiratory Syndrome Coronavirus. ChemBioEng Reviews. (2): 118–132.
- 36. Lei et al, 2018. Nsp3 of coronaviruses: Structures and functions of a large multi-domain protein. Antiviral Research. 149: 58–74.
- 37. Lin et al, 2013. Full genome analysis of a novel type II feline coronavirus NTU156. Virus Genes 46: 316–322.
- 38. Lipinski et al, 2001. Experimental and Computational Approaches to Estimate Solubility and Permeability in Drug Discovery and Development Settings. Advanced Drug Delivery Reviews. 23: 3–25.
- 39. Lohèzic-Le Dèvèhat et al, 2007. Stictic acid derivatives from the lichen Usnea articulata and their antioxidant activities. Journal of Natural Products. 70(7): 1218–1220.
- 40. Manasateinkij et al, 2009. Occurrence of feline coronavirus and feline infectious peritonitis virus in Thailand. Kasetsart journal (Natural Science) 43: 720–726.
- 41. Milne et al, 2002. Depsides and Depsidones as Inhibitors of HIV-1 Integrase: Discovery of Novel Inhibitors through 3D Database Searching. Journal of Medicinal Chemistry. 40(6): 942–951.
- 42. Miyanaga et al, 2016. Identification of the fluvirucin B2(Sch 38518) biosynthetic gene cluster from actinomadura fulva sub sp. Indica ATCC 53714: Substrate Specificity of the β -amino acid selective adenylating enzyme FlvN. Bioscience, Biotechnology and Biochemistry. 80(5): 935–941.

- 43. Murkherjee et al, 2011. Inhibitor of SAR-3CLpro: Virtual screening, biological evaluation, and molecular dynamics simulation studies. Journal of Chemical information and Modeling. 51: 1376–1392.
- 44. Naruse et al, 1991a. Fluvirucins A1, A2, B1, B2, B3, B4 and B5, new antibiotics active against influenza a virus. I. production, isolation, chemical properties and biological activities. J. Antibiot. 44: 733–740.
- 45. Naruse et al, 1991b. Fluvirucins A1, A2, B1, B2, B3, B4 and B5, new antibiotics active against influenza a virus. III. The stereochemistry and absolute configuration of fluvirucin A1. J. Antibiot. 44: 756–761.
- 46. Neamati et al, 1997. Depsides and Depsidones as Inhibitors of HIV-1 Integrase: Discovery of Novel Inhibitors through 3D Database Searching. Journal of Medicinal Chemistry. 40(6): 942–951.
- 47. Niu et al, 2008. Molecular docking identifies the binding of 3-chloropyridine moieties specifically to the S1 pocket of SARS-CoV Mpro. Bioorganic & Medicinal Chemistry. 16: 293–302.
- 48. Noel et al, 2011. Open Babel: An open chemical toolbox. J. Cheminf. 3: 33.
- 49. Omer and Singh, 2017. An integrated approach of network-based systems biology, molecular docking, and molecular dynamics approach to unravel the role of existing antiviral molecules against AIDS-associated cancer. Journal of Biomolecular Structure and Dynamics. 35(7): 1547–1558.
- 50. Omrani et al, 2014. Ribavirin and interferon alfa-2a for severe Middle East respiratory syndrome coronavirus infection: A retrospective cohort study. The Lancet Infectious Diseases. 14(11): 1090–1095.Morris et al, 2009. AutoDock4 and AutoDockTools4: Automated docking with selective receptor flexibility. J. Comput. Chem. 30: 2785-2791.
- 51. Oprea, 2000. Current trends in lead discovery: Are we looking for the appropriate properties? Molecular Diversity. 5(4): 199–208.
- 52. Papadopoulou et al, 2007. Beta-orcinol metabolites from the lichen Hypotrachyna revoluta. Molecules. 12: 997–1005.
- 53. Pedersen et al, 2007. Significance of coronavirus mutants in feces and diseased tissues of cats suffering from feline infectious peritonitis. Viruses. 1:166-184.
- 54. Pedersen NC, 2009. A review of feline infectious peritonitis virus infection: 1963–2008. Journal of Feline Medicine and Surgery. 11: 225–258.
- 55. Pedersen NC, 2014b. An update on feline infectious peritonitis: virology and immunopathogenesis. The Veterinary Journal. 201:123–132.

- 56. Pedersen NC, 2014a. An update on feline infectious peritonitis: diagnostics and therapeutics. The Veterinary Journal. 201: 133–141.
- 57. Pedersen and Black, 1983. Attempted immunization of cats against feline infectious peritonitis, using avirulent live virus or sublethal amounts of virulent virus. American Journal of Veterinary Research. 44: 229–234.
- 58. Perola et al, 2007. Comments on the article "On evaluating molecular-docking methods for pose prediction and enrichment factors". J Chem Inf Model. 47(2): 251-253.
- 59. Reed and Munech, 1938. A simple method of estimating fifty percent endpoints. American Journal of Hygiene. 27: 493–497.
- 60. Sander et al, 2015. DataWarrior: An open-source program for chemistry aware data visualization and analysis. Journal of Chemical Information and Modeling. 55(2): 460–473.
- 61. Salentin et al, 2015 PLIP: fully automated protein-ligand interaction profiler. Nucl. Acids Res. 43 (W1): W443-W447.
- 62. Scott et al, 1995. Independent evaluation of a modified live FIPV vaccine under experimental conditions (Cornell experience). Feline Practice. 23:74–76.
- 63. Shie et al, 2005. Inhibition of the severe acute respiratory syndrome 3CL protease by peptidomimetic α , β -unsaturated esters. Bioorganic & Medicinal Chemistry. 13: 5240–5252.
- 64. Severson, 2007. Development and validation of a high-throughput screen for inhibitors of SARS CoV and its application in screening of a 100,000-compound library. Journal of Biomolecular Screening. 12(1): 33–40.
- 65. Singh et al, 2003. Four novel bis-(naphtho-γ-pyrones) isolated from Fusarium species as inhibitors of HIV-1 integrase. Bioorganic and Medicinal Chemistry Letters. 13(4): 713–717.
- 66. Simons et al, 2005. A mRNA PCR for the diagnosis of feline infectious peritonitis. Journal of Virological Methods. 124:11–116.
- 67. St. John et al, 2015. X-ray structure and inhibition of the feline infectious peritonitis virus 3C-like protease: structure implications for drug design. Bioorganic & Medicinal Chemistry Letters. 25: 5072–5077.
- 68. Tiew et al, 2011. Design, synthesis, and evaluation of inhibitors of Norwalk virus 3C protease. Bioorganic and Medicinal Chemistry Letters. 21(18): 5315–5319.
- 69. Triballeau et al, 2005. Virtual screening workflow development guided by the "receiver operating characteristic" curve approach. Application to high-throughput docking on metabotropic glutamate receptor subtype 4. J Med Chem. 48: 2534-47.

- 70. Trott O and Olson AJ 2010. AutoDock Vina: improving the speed and accuracy of docking with a new scoring function, efficient optimization, and multithreading. Journal of Computational Chemistry. 31: 455–461.
- 71. Turner, 2005. XMGRACE, Version 5.1.19. Center for Coastal and Land-Margin Research, Oregon Graduate Institute of Science and Technology, Beaverton, OR.
- 72. Umezawa, et al, 1981. A new antitumor antibiotic, stubomycin. J. Antibiot. 34: 259 –265.
- 73. Ugaki et al, 2012. New isochaetochromin, an inhibitor of triacylglycerol synthesis in mammalian cells, produced by Penicillium sp. FKI-4942: II. structure elucidation. Journal of Antibiotics. 65(1): 21–24.
- 74. Wang et al, 2015. Crystal structure of feline infectious peritonitis virus main protease in complex with synergistic dual inhibitors. Journal of Virology. 90(4): 1910–1916.
- 75. Wang and Wang, 2002. How Does Consensus Scoring Work for Virtual Library Screening? An Idealized Computer Experiment. Journal of Chemical Information and Computer Sciences. 41(5): 1422–1426.
- 76. Wassman et al, 2013. Computational identification of a transiently open L1/S3 pocket for reactivation of mutant p53. Nature Communications. 4: 1–9.
- 77. Weiss et al, 1993. Toxicologic effects of ribavirin in cats. Journal of Veterinary Pharmacology Therapeutics. 16: 301–316.
- 78. White et al, 2014. Antioxidant Activity and Mechanisms of Action of Natural Compounds Isolated from Lichens: A Systematic Review. Molecules. 19(9): 14496–14527.
- 79. Wu et al, 2004. Small molecules targeting severe acute respiratory syndrome human coronavirus. PNAS. 101(27): 10012–10017.
- 80. Zhang et al, 2017. Virtual screening approach to identifying influenza virus neuraminidase inhibitors using molecular docking combined with machine-learning-based scoring function. Oncotarget. 8(47), 83142–83154.
- 81. Zhao et al, 2009. A statistical framework to evaluate virtual screening. BMC Bioinformatics. 10: 225.
- 82. Zhou et al, 2006. Isatin compounds as noncovalent SARS coronavirus 3Clike protease inhibitors. J Med Chem. 49: 3440–3443.
- 83. Zumla et al, 2016. Coronaviruses drug discovery and therapeutic options. Nat Rev Drug Discov.15(5): 327-347.